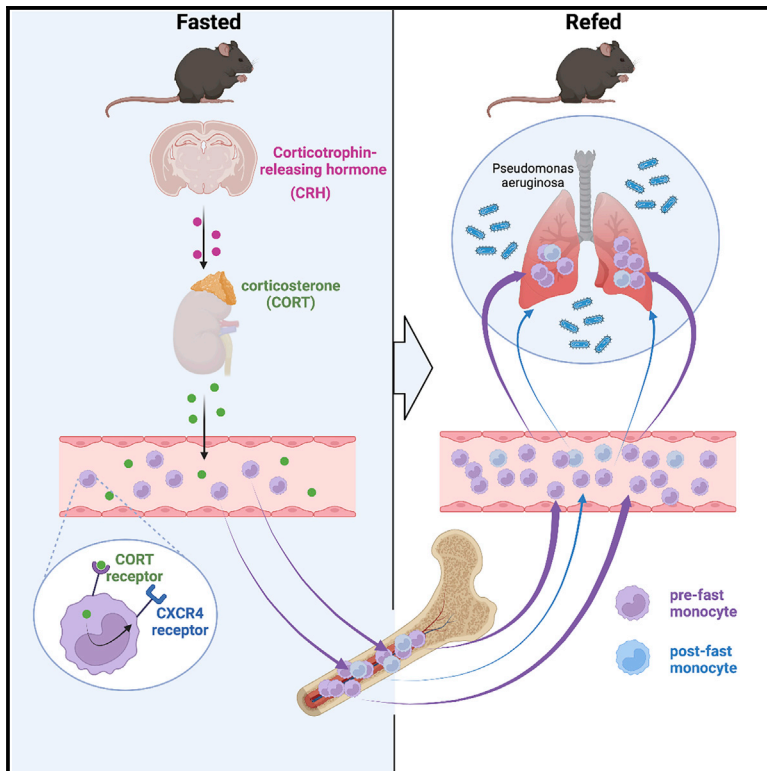


Immunity

Monocytes re-enter the bone marrow during fasting and alter the host response to infection

Graphical abstract



Authors

Henrike Janssen, Florian Kahles, Dan Liu, ..., Miriam Merad, Matthias Nahrendorf, Filip K. Swirski

Correspondence

filip.swirski@mssm.edu

In brief

Fasting influences the distribution of leukocytes throughout the body, but its mechanisms and implications are only partly understood. Here, Janssen et al. reveal how fasting leads to homing of monocytes into the bone marrow. Re-feeding gives rise to a surge of circulating monocytes with deleterious effects on bacterial host response.

Highlights

- Circulating monocytes migrate to the bone marrow upon fasting
- Monocytes augment CXCR4 via a fasting-induced hormonal stress response
- Re-feeding after prolonged fasting results in a surge of monocytes into circulation
- Prolonged fasting and re-feeding alter the immune response to bacterial infection

Article

Monocytes re-enter the bone marrow during fasting and alter the host response to infection

Henrike Janssen,^{1,2,8} Florian Kahles,^{2,8} Dan Liu,² Jeffrey Downey,^{1,2} Laura L. Koekkoek,¹ Vladimir Roudko,³ Darwin D'Souza,³ Cameron S. McAlpine,^{1,2} Lennard Halle,² Wolfram C. Poller,^{1,2} Christopher T. Chan,^{1,2} Shun He,² John E. Mindur,² Máté G. Kiss,^{1,2} Sumnima Singh,^{1,2} Atsushi Anzai,² Yoshiko Iwamoto,² Rainer H. Kohler,² Kashish Chetal,⁴ Ruslan I. Sadreyev,⁴ Ralph Weissleder,^{2,5,6} Seunghee Kim-Schulze,^{3,7} Miriam Merad,^{1,3,7} Matthias Nahrendorf,^{2,5} and Filip K. Swirski^{1,2,7,9,*}

¹Cardiovascular Research Institute, Icahn School of Medicine at Mount Sinai, New York, NY, USA

²Center for Systems Biology, Massachusetts General Hospital and Harvard Medical School, Boston, MA, USA

³Human Immune Monitoring Center, Icahn School of Medicine at Mount Sinai, New York, NY, USA

⁴Department of Molecular Biology and Department of Pathology, Massachusetts General Hospital and Harvard Medical School, Boston, MA, USA

⁵Department of Radiology, Massachusetts General Hospital and Harvard Medical School, Boston, MA, USA

⁶Department of Systems Biology, Harvard Medical School, Boston, MA, USA

⁷Marc and Jennifer Lipschultz Precision Immunology Institute, Icahn School of Medicine at Mount Sinai, New York, NY, USA

⁸These authors contributed equally

⁹Lead contact

*Correspondence: filip.swirski@mssm.edu

<https://doi.org/10.1016/j.immuni.2023.01.024>

SUMMARY

Diet profoundly influences physiology. Whereas over-nutrition elevates risk for disease via its influence on immunity and metabolism, caloric restriction and fasting appear to be salutogenic. Despite multiple correlations observed between diet and health, the underlying biology remains unclear. Here, we identified a fasting-induced switch in leukocyte migration that prolongs monocyte lifespan and alters susceptibility to disease in mice. We show that fasting during the active phase induced the rapid return of monocytes from the blood to the bone marrow. Monocyte re-entry was orchestrated by hypothalamic-pituitary-adrenal (HPA) axis-dependent release of corticosterone, which augmented the CXCR4 chemokine receptor. Although the marrow is a safe haven for monocytes during nutrient scarcity, re-feeding prompted mobilization culminating in monocytosis of chronologically older and transcriptionally distinct monocytes. These shifts altered response to infection. Our study shows that diet—in particular, a diet's temporal dynamic balance—modulates monocyte lifespan with consequences for adaptation to external stressors.

INTRODUCTION

Caloric excess reduces organismal lifespan,^{1–3} increases systemic inflammation,^{4,5} elevates risk for cardiometabolic diseases,^{4,6} and exacerbates bacterial infection.^{3,7} Conversely, caloric restriction and fasting have been shown to inversely correlate with hypertension, atherosclerosis, diabetes, obesity, colitis, asthma, and psoriasis.^{8–12} As ingested energy sources engage with multiple metabolic processes that affect physiology, the precise mechanisms linking diet with tissue, cellular, and molecular function remain poorly understood.

Recent studies have indicated that diet influences the distribution of leukocytes throughout the body. For example, Belkaid and colleagues showed that T lymphocytes relocate from secondary lymphoid organs to the bone marrow (BM) during caloric restriction,¹³ Hase and colleagues discovered that B cells leave Peyer's patches,¹⁴ while Merad and colleagues have demonstrated that fasting reduces the number of circulating monocytes

in mice and humans by preventing their mobilization from the BM.¹⁵ All studies reveal that diet-dependent shifts in leukocyte distribution can have major effects on disease outcome and, in particular, to the response during infection, oral tolerance, tumor growth, and experimental autoimmune encephalomyelitis. These insights raise a number of fundamental questions concerning diet's control of leukocyte biology. As dietary restriction leads to hunger, it remains unclear how the brain participates in these phenomena, particularly in light of recent studies on the central nervous system's regulation of peripheral leukocytes.^{16,17} Moreover, the fate of leukocytes during fasting is unclear: for example, monocytes are typically short-lived, raising the question as to whether fasting influences their lifespan, production, and death. Unless fasting continues to starvation, it is followed by re-feeding, the consequences of which are unknown. In this study we focused on the mechanism and effects of fasting and re-feeding on monocyte dynamics and homeostasis.

Table 1. Absolute counts of major leukocyte populations in selected organs in mice continuously fed or fasted for 24 h

	Monocytes		Neutrophils	
	Fed	24-h fast	Fed	24-h fast
Blood ($\times 10^3$ cells/mL)	724 \pm 212 n = 5	37 \pm 14 n = 5, p < 0.05	1,539 \pm 291 n = 4	424 \pm 38 n = 4, p < 0.05
Spleen ($\times 10^3$ cells/organ)	185 \pm 7.7 n = 3	14 \pm 2.0 n = 3, p < 0.001	191 \pm 20 n = 3	82 \pm 26 n = 3, p < 0.05
Liver ($\times 10^4$ cells/organ)	7.0 \pm 0.4 n = 3	0.6 \pm 0.2 n = 3, p < 0.001	8.5 \pm 0.7 n = 3	4.9 \pm 3.0 n = 3, p = n.s.
Lung ($\times 10^3$ cells/organ)	148 \pm 32 n = 3	31 \pm 3.7 n = 3, p < 0.05	150 \pm 20 n = 3	67 \pm 11 n = 3, p < 0.05
WAT (cells/organ)	626 \pm 247 n = 3	61 \pm 14 n = 3, p = n.s.	2,104 \pm 997 n = 4	379 \pm 79 n = 4, p = n.s.
BAT ($\times 10^3$ cells/organ)	2.1 \pm 0.4 n = 4	0.6 \pm 0.3 n = 4, p < 0.05	6.8 \pm 2.4 n = 4	3.3 \pm 0.9 n = 4, p = n.s.
Heart ($\times 10^3$ cells/organ)	2.0 \pm 0.2 n = 3	1.4 \pm 0.4 n = 3, p = n.s.	2.4 \pm 0.6 n = 3	3.1 \pm 0.4 n = 3, p = n.s.
Muscle (cells/mg)	1.7 \pm 0.3 n = 5	0.9 \pm 0.3 n = 4, p = n.s.	1.8 \pm 0.3 n = 5	4.7 \pm 2.3 n = 5, p = n.s.
Pancreas ($\times 10^3$ cells/organ)	1.8 \pm 0.6 n = 5	0.9 \pm 0.2 n = 5, p = n.s.	1.2 \pm 0.2 n = 5	0.4 \pm 0.1 n = 5, p < 0.05
SI lamina propria ($\times 10^3$ cells/organ)	2.9 \pm 0.5 n = 3	1.0 \pm 0.2 n = 3, p < 0.05	0.9 \pm 0.3 n = 4	1.7 \pm 0.6 n = 5, p = n.s.
LI lamina propria ($\times 10^3$ cells/organ)	0.7 \pm 0.2 n = 4	0.6 \pm 0.3 n = 4, p = n.s.	0.8 \pm 0.2 n = 4	0.6 \pm 0.2 n = 4, p = n.s.
MLN ($\times 10^3$ cells/LN)	0.27 \pm 0.03 n = 4	0.06 \pm 0.01 n = 4, p < 0.001	0.26 \pm 0.01 n = 4	0.13 \pm 0.03 n = 4, p < 0.01
Peyer patches ($\times 10^3$ cells/PP)	0.028 \pm 0.017 n = 5	0.006 \pm 0.002 n = 5, p = n.s.	0.004 \pm 0.001 n = 5	0.001 \pm 0.0002 n = 5, p < 0.01
Peritoneum ($\times 10^3$ cells/organ)	1.9 \pm 0.4 n = 3	0.8 \pm 0.1 n = 4, p < 0.05	1.0 \pm 0.7 n = 3	0.6 \pm 0.3 n = 4, p = n.s.
Mesenteric AT ($\times 10^3$ cells/organ)	8.8 \pm 1.6 n = 3	0.8 \pm 0.1 n = 3, p < 0.01	3.1 \pm 1.4 n = 3	1.2 \pm 0.2 n = 3, p = n.s.
Bone marrow ($\times 10^4$ cells/femur)	13 \pm 1.1 n = 3	18 \pm 0.8 n = 3, p < 0.05	105 \pm 8.8 n = 3	107 \pm 6.5 n = 3, p = n.s.
			T cells	B cells
			Fed	24-h fast
Blood ($\times 10^3$ cells/mL)	1,409 \pm 181 n = 4	760 \pm 106 n = 4, p < 0.05	4,619 \pm 396 n = 4	2,138 \pm 253 n = 4, p < 0.01
Spleen ($\times 10^3$ cells/organ)	8,498 \pm 1,317 n = 3	6,790 \pm 337 n = 3, p = n.s.	18,010 \pm 1,703 n = 3	12,686 \pm 1,391 n = 3, p = n.s.
Liver ($\times 10^4$ cells/organ)	57 \pm 9.6 n = 3	36 \pm 12 n = 3, p = n.s.	191 \pm 30 n = 3	96 \pm 46 n = 3, p = n.s.
Lung ($\times 10^3$ cells/organ)	598 \pm 77 n = 3	280 \pm 61 n = 3, p < 0.05	1,007 \pm 85 n = 3	459 \pm 61 n = 3, p < 0.01
WAT (cells/organ)	16,967 \pm 5,009 n = 4	4,099 \pm 1,278 n = 4, p = n.s.	2,437 \pm 551 n = 4	621 \pm 175 n = 4, p < 0.05
BAT ($\times 10^3$ cells/organ)	9.9 \pm 2.0 n = 4	4.3 \pm 0.6 n = 4, p < 0.05	14 \pm 3.8 n = 4	5.4 \pm 1.6 n = 4, p = n.s.
Heart ($\times 10^3$ cells/organ)	3.8 \pm 0.8 n = 3	2.8 \pm 0.3 n = 3, p = n.s.	15 \pm 2.4 n = 3	6.9 \pm 0.9 n = 3, p < 0.05

(Continued on next page)

Table 1. Continued

	T cells		B cells	
	Fed	24-h fast	Fed	24-h fast
Muscle (cells/mg)	3.5 ± 0.6 n = 5	4.4 ± 1.9 n = 5, p = n.s.	4.7 ± 0.9 n = 5	11 ± 6.6 n = 5, p = n.s.
Pancreas (×10 ³ cells/organ)	12 ± 3.2 n = 5	59 ± 25 n = 5, p = n.s.	11 ± 4.3 n = 5	59 ± 27 n = 5, p = n.s.
SI lamina propria (×10 ³ cells/organ)	17 ± 5.3 n = 4	103 ± 17 n = 5, p < 0.01	105 ± 52 n = 4	460 ± 123 n = 5, p = n.s.
LI lamina propria (×10 ³ cells/organ)	22 ± 4.1 n = 4	21 ± 3.6 n = 4, p = n.s.	114 ± 37 n = 4	52 ± 11 n = 4, p = n.s.
MLN (×10 ³ cells/LN)	239 ± 25 n = 4	130 ± 4.4 n = 4, p < 0.01	211 ± 27 n = 4	96 ± 8.2 n = 4, p < 0.01
Peyer patches (×10 ³ cells/PP)	8.9 ± 0.7 n = 5	4.2 ± 0.4 n = 5, p < 0.001	51 ± 14 n = 5	30 ± 4.5 n = 5, p = n.s.
Peritoneum (×10 ³ cells/organ)	26 ± 3.4 n = 3	54 ± 11 n = 4, p = n.s.	246 ± 40 n = 3	353 ± 63 n = 4, p = n.s.
Mesenteric AT (×10 ³ cells/organ)	25 ± 7.2 n = 3	17 ± 0.9 n = 3, p = n.s.	9.1 ± 1.4 n = 3	6.3 ± 1.3 n = 3, p = n.s.
Bone marrow (×10 ⁴ cells/femur)	2.5 ± 0.2 n = 3	9.2 ± 1.4 n = 3, p < 0.05	173 ± 4.6 n = 3	166 ± 9.4 n = 3, p = n.s.

Unpaired t test. Data presented as mean ± SEM, *p < 0.05, **p < 0.01, ***p < 0.001. (WAT, white adipose tissue; BAT, brown adipose tissue; SI, small intestine; LI, large intestine; MLN, mesenteric lymph nodes; AT, adipose tissue). Please also see [Figure 1](#).

RESULTS

Fasting reorganizes the leukocyte-distribution landscape

We started our study by enumerating major leukocyte classes (B and T lymphocytes, monocytes, and neutrophils) across 16 organs and tissues in response to a 24-h fast. Our data tabulated ([Tables 1](#) and [S1](#)) and represented graphically ([Figures 1A](#) and [1B](#)), illustrate major and rapid shifts for each leukocyte type. Whereas some tissues experienced an increase, others saw a decrease in leukocyte numbers after fasting. Notably, every tissue except the BM had a reduced number of Ly-6C^{hi} monocytes compared with the corresponding tissue of non-fasted animals, which is consistent with recent work in both mice and humans.¹⁵ The relative increase of monocytes in the BM after a 24-h fast is likewise consistent with the idea that fasting prevents monocyte mobilization from the BM to the blood.¹⁵

Monocyte numbers in the blood fluctuate according to circadian rhythms.¹⁸ In mice, monocyte numbers peak in the blood during the day shortly after mice go to sleep (approximately 6 h after the start of the fast, i.e., ~zeitgeber [ZT]6) and reach their nadir at night shortly after mice wake up (~ZT16). The mechanisms that control this circadian rhythm are incompletely understood.^{19,20} We performed a time-course analysis, asking whether the fasting effect on Ly-6C^{hi} monocytes depended on the time of day. We found that food restriction during the active period (ZT12–ZT24/0) but not during the inactive period (ZT0–ZT12), rapidly reduced blood-glucose concentration, and circulating Ly-6C^{hi} monocytes, suggesting that meals early after waking prevent drops in leukocyte numbers ([Figure 1C](#)). We found similar patterns for neutrophils, T cells, and B cells.

Fasting returns Ly-6C^{hi} monocytes back from circulation to the BM

Having documented a decrease of monocytes in the periphery—including the blood, which we verified with intravital microscopy ([Figure S1A](#); [Videos S1](#) and [S2](#))—along with a corresponding increase in the BM, we next sought to identify the relevant mechanism. Earlier work suggested that a fasting-mediated mobilization shutdown from the BM drives this phenomenon.¹⁵ However, we speculated there may be additional mechanisms. First, Ly-6C^{hi} monocytes disappeared from the blood 4 h after food deprivation in the active period ([Figure 1C](#)). This appeared to be much faster than expected. Under the assumptions that fasting leads to a complete shutdown of BM Ly-6C^{hi} monocyte egress and that a typical half-life of circulating Ly-6C^{hi} monocytes of approximately 20 h,²¹ the expected reduction of blood monocytes after a 20-h fast, in the absence of any additional mechanisms would be ~50% ([Figure S1B](#)). However, we observed a ~90% reduction of circulating Ly-6C^{hi} monocytes in mice after only 4 h, suggesting the contribution of additional mechanisms beyond bone-marrow monocyte egress ([Figure 1C](#)). Second, mice lacking *Ccr2*, the chemokine receptor responsible for mobilization from the BM, also experienced a fasting monocyte phenotype ([Figure S1C](#)). The caveat that these mice already have reduced monocyte numbers in the blood at steady state notwithstanding, the data nevertheless point to a mobilization-independent mechanism. Third, we excluded several candidate mechanisms, noting that the disappearance of Ly-6C^{hi} monocytes in response to fasting was independent of CD18/LFA1 and CX3CR1-mediated patrolling behavior ([Figure S1C](#)) and independent of myeloid-derived (5'AMP-activated protein kinase) AMPK (*Prkaa1*), the clock gene *Arntl*, and Glut-1 (*Slc2a1*)

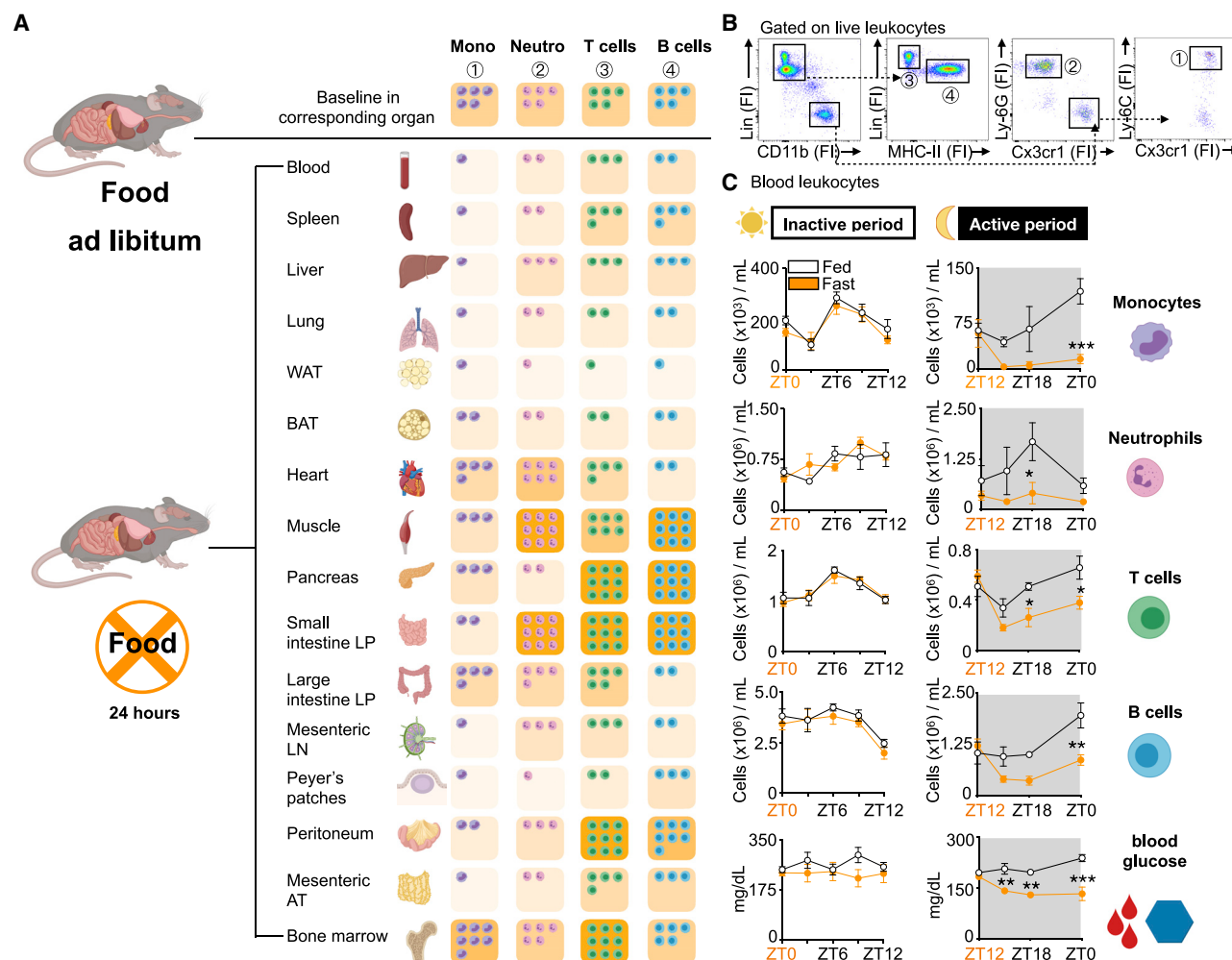


Figure 1. Fasting reorganizes the leukocyte-distribution landscape

(A) Relative shifts of major leukocyte populations in depicted organs compared between mice fed *ad libitum* and after a 24-h fast. Baseline cell content in each organ is defined as “5 cells.” Fasted results are calculated in relative relation to fed controls. Ly-6C^{hi} monocytes are defined as CD45⁺ CD11b⁺ LIN1⁻ CD19, CD3, NK 1.1, CD90⁻ Ly-6G⁻ CX3CR1⁺ Ly-6C^{hi}; neutrophils as CD45⁺ CD11b⁺ LIN1⁻ Ly-6G⁺; T cells as CD45⁺ CD11b⁻ LIN1⁺ MHCII⁻; B cells as CD45⁺ CD11b⁻ LIN1⁺ MHCII⁺. Absolute numbers for each organ are depicted in Table 1. (n = 3–5 mice per group; unpaired t test.)

(B) Representative gating strategy of all major leukocyte populations in the blood.

(C) Absolute blood-leukocyte count and blood-glucose concentration divided by inactive (light) and active (dark) periods compared between mice fed *ad libitum* or fasted for up to 12 h. Orange zeitgeber (ZT) indicates start of the fast (n = 3–10 per group). Two-way ANOVA. Data presented as mean \pm SEM; *p < 0.05, **p < 0.01, ***p < 0.001. Mono, Ly-6C^{hi} monocytes; Neutro, neutrophils; WAT, white adipose tissue; BAT, brown adipose tissue; LP, lamina propria; LN, lymph node; AT, adipose tissue; Fl, fluorescence intensity; ZT, zeitgeber.

See also Tables 1 and S1.

(Figure S1D). Moreover, the disappearance of Ly-6C^{hi} monocytes in response to fasting was not caused by monocyte-platelet aggregation (Figure S1E), was independent of T or B cells (Figure S1F), and it occurred in aged mice (Figure S1G) and in both sexes (Figure S1G), and different genetic backgrounds (Figure S1H). When mice were fasted for 24 h every other day for a period of 2 weeks, the effect persisted (Figure S1I) and was therefore not subjected to adaptation.

We elected to conduct a pulse-chase experiment involving the adoptive transfer of GFP⁺ monocytes to either fed or fasted mice (Figure 2A). After transfer and 24 h of fasting, a GFP⁺ monocyte population was present in the blood of fed mice, but absent in the blood of fasted mice (Figures 2B and 2D). As hypothesized, it

was the BM of fasted mice that not only contained the transferred GFP⁺ cells, but contained more of them compared with the *ad libitum*-fed group (Figures 2C and 2D). Because GFP⁺ monocytes were transferred intravenously, their appearance in the BM necessarily required migration from blood to the BM. The adoptive transfer experiments suggested that reverse mobilization (i.e., the migration of monocytes from the blood to the BM) is an important mechanism contributing to the fasting-induced phenomenon.

To explore the reverse mobilization idea mechanistically, we measured a cassette of potentially relevant genes, such as clock genes and genes important to leukocyte adhesion and migration, on monocytes retrieved from the blood of fasted and fed

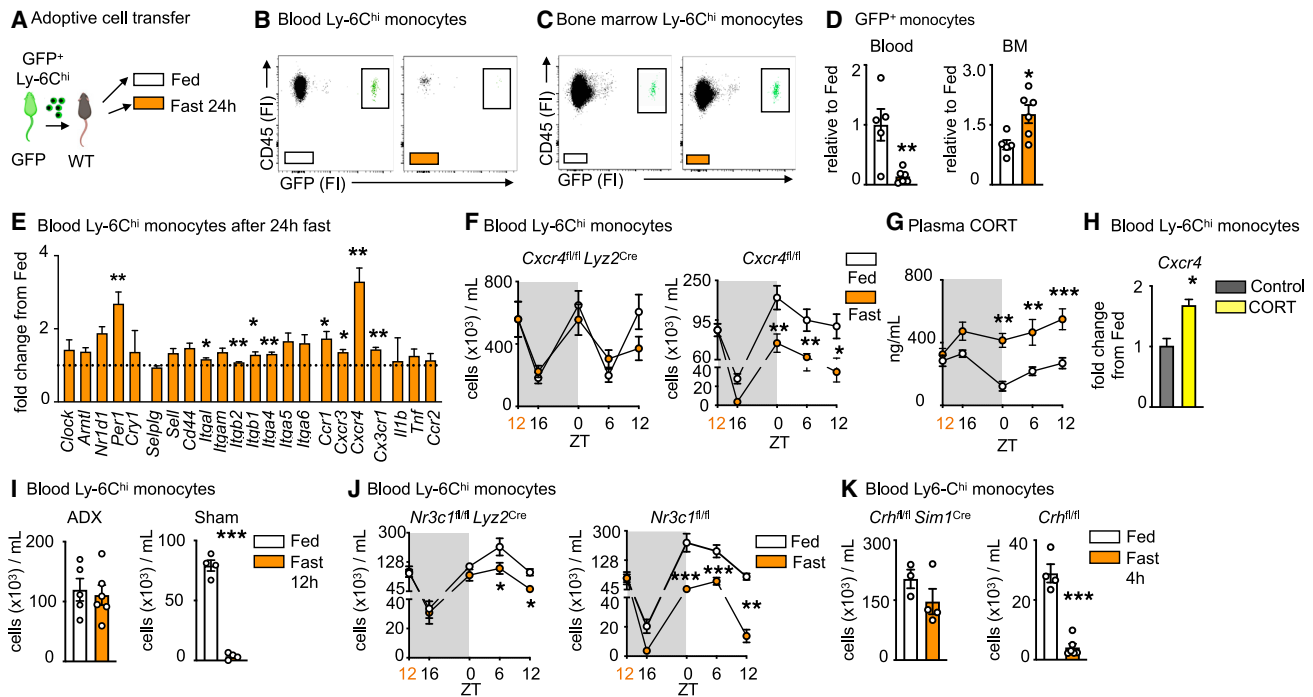


Figure 2. Fasting returns Ly-6C^{hi} monocytes back from circulation to the bone marrow

(A) Ly-6C^{hi} monocytes isolated from GFP-positive mice were injected intravenously into wild-type mice directly prior to initiation of a 24-h fast or feeding *ad libitum*.
 (B) Representative flow-cytometry plots of GFP-positive monocytes in the blood after feeding *ad libitum* and fasting. Adoptively transferred monocytes are defined as CD45⁺ GFP⁺. (n = 5–6 per group; two independent experiments combined.)
 (C) Representative flow-cytometry plots of GFP-positive monocytes in the bone marrow (BM) after feeding *ad libitum* and fasting. Adoptively transferred monocytes are defined as CD45⁺ GFP⁺. (n = 5–6 per group, two independent experiments combined.)
 (D) Relative decrease of GFP-positive monocytes in the blood and relative increase of GFP-positive monocytes in the bone marrow after 24 h of fasting compared with fed control (n = 5–6 per group; two independent experiments combined; unpaired t test).
 (E) Relative expression of target genes of sorted blood Ly-6C^{hi} monocytes after 24 h of fasting normalized to fed control. (n = 3 mice per group; unpaired t test.)
 (F) Circulating Ly-6C^{hi} monocytes measured at indicated time points in *Cxcr4*^{fl/fl} *Lyz2*^{Cre} and *Cxcr4*^{fl/fl} under fed and fasted conditions (n = 4–10; time points are independent experiments). Start of the fast is indicated by orange zeitgeber (ZT). Two-way ANOVA.
 (G) Plasma corticosterone (CORT) in *Cxcr4*^{fl/fl} under fed and fasted conditions at indicated time points (n = 4–8, time points are independent experiments). Start of the fast is indicated by orange zeitgeber (ZT). Two-way ANOVA.
 (H) Relative expression of *Cxcr4* on sorted blood Ly-6C^{hi} monocytes after incubation with CORT (n = 10 mice pooled for sort, n = 3 technical replicates per group; unpaired t test).
 (I) Mice underwent bilateral adrenalectomy (ADX) or sham surgery and were allowed to recover for 2 weeks prior to submission to feeding *ad libitum* or a 12-h fast. Blood Ly-6C^{hi} monocytes in mice 2 weeks post-ADX or sham surgery after fasting compared with fed *ad libitum* (n = 4–6 per group; unpaired t test).
 (J) Blood Ly-6C^{hi} monocytes measured at indicated times in *Nr3c1*^{fl/fl} *Lyz2*^{Cre} and *Nr3c1*^{fl/fl} under fed and fasted conditions (n = 4–11, time points are independent experiments). Start of the fast is indicated by orange ZT. Two-way ANOVA.
 (K) Blood Ly-6C^{hi} monocytes in *Crh*^{fl/fl} *Sim1*^{Cre} and *Crh*^{fl/fl} after 4 h of fasting compared with fed *ad libitum* (n = 3–6 per group; unpaired t test. Data presented as mean ± SEM; *p < 0.05, **p < 0.01, ***p < 0.001). FI, fluorescence intensity; BM, bone marrow; CORT, corticosterone; ADX, adrenalectomy.
 See also [Figure S1](#).

mice (Figure 2E). Among transcripts measured, *Cxcr4* was particularly notable because it was expressed nearly 4-fold above fed conditions and because it is known to facilitate medullary-cell retention, as the loss of *Cxcr4* expression mobilizes leukocytes to the blood.¹⁸ We therefore generated mice lacking *Cxcr4* on myeloid cells. The rapid and lasting fasting-induced monocytopenia in controls was abolished in the absence of *Cxcr4* (Figures 2F and S1J), without affecting the typical circadian fluctuations that are known to be controlled by the circadian clocks.¹⁸ The data provide further evidence for reverse migration of monocytes from the blood to the BM.

Previous studies from us and others have shown that corticosterone (CORT) augments *Cxcr4* expression.^{17,22} We therefore

wondered whether CORT was responsible for the phenomenon. We first observed that fasting rapidly and consistently increased CORT in the blood (Figure 2G), which is in keeping with the idea that fasting induces a CORT-mediated stress-like response. The addition of CORT to sorted monocytes *in vitro* increased *Cxcr4* expression (Figure 2H), and adrenalectomy (ADX)—which prevented a CORT spike in response to fasting (Figure S1K)—also prevented monocytopenia (Figure 2I) and led to an increase of Ly-6C^{hi} monocytes in the BM (Figure S1L). Fasting is known to increase plasma free-fatty acids via lipolysis of adipose tissue (AT).²³ This partly depends on the melanocortin-3 receptor and thereby on the activation of the hypothalamic-pituitary-adrenal (HPA) axis.²⁴ We found that fasted and adrenalectomized mice

developed severe hypoglycemia with no weight loss and no change in plasma fatty acids (Figures 2O and S1M). These observations led us to ask whether CORT was directly engineering reverse mobilization or if this was a phenomenon induced by another mechanism downstream of the adrenal gland. We deleted the glucocorticoid receptor (*Nr3c1*) from myeloid cells and indeed discovered that fasting no longer induced the disappearance of monocytes from the blood in those mice (Figures 2J and S1P).

CORT, produced by the adrenal glands, is an end product of the HPA axis, which originates in the paraventricular hypothalamus (PVH) containing a small cluster of corticotropin-releasing hormone (CRH) neurons. To determine whether mass migration of monocytes from the blood to the BM was controlled by this cluster—as opposed to other possible mechanisms that converge on CORT production—we generated mice with cell-specific deletion of *Crh* in neurons of the hypothalamus (*Crh^{fl/fl} Sim1^{Cre}*). Compared with controls, we did not detect monocytopenia in fasted mice lacking CRH expression (Figure 2K). To confirm that the lack of fasting-induced monocytopenia was indeed a result of an impaired HPA-axis response, we injected *Crh^{fl/fl} Sim1^{Cre}* and littermate controls with CORT (Figure S1Q). Hypercorticosteronemia increased CXCR4 and reduced circulating monocytes in *Crh^{fl/fl} Sim1^{Cre}* and *Crh^{fl/fl}* mice (Figures S1R and S1S). Thus, monocyte reverse-medullary migration during fasting is controlled by a hypothalamic brain axis that induces monocytic CXCR4 expression via direct CORT engagement.

Re-feeding leads to a surge of monocytes into the bloodstream

Seclusion of monocytes in the BM during fasting raises questions as to their fate. Rather than exploring how even more severe fasting, which would lead to starvation and eventual death, affects monocytes, we wondered how circulating monocyte numbers would change upon re-feeding. We anticipated that monocytes would re-enter the blood, but could not surmise how quickly this would happen and to what extent. We therefore enumerated circulating monocytes in mice that were fed *ad libitum*, fasted, or fasted and re-fed (Figure 3A). Next to the characteristic monocytopenia in fasted conditions, mice that were re-fed developed monocytosis 4 h after re-feeding, dwarfing the typical monocyte numbers found in *ad libitum*-fed mice at this stage of the circadian clock (Figures 3B and 3C). We observed a similar, if slightly muted, surge among neutrophils, but not among lymphocytes (Figure S2A). The monocytic surge correlated with blood glucose (Figure 3D) and inversely correlated with plasma CORT (Figure 3E). The data point to a robust liberation of sequestered monocytes into the blood shortly after food reintroduction.

To chart mobilization more directly, we performed two types of cell tracking experiments. First, we adoptively transferred GFP⁺ monocytes to mice that were subsequently fasted or fasted and re-fed (Figure 3F). Similar to our prior experiment, we noted slightly more monocytes in blood and fewer monocytes in BM of re-fed mice, suggesting mobilization after re-feeding (Figure 3G). These reappearing GFP⁺Ly-6C^{hi} monocytes upon re-feeding were alive and not eaten by endogenous GFP⁻Ly-6C^{hi} monocytes (Figure S2B). Second, we supplemented this experiment with the use of parabiosis, partnering GFP⁺ mice with wild-type mice for 2 weeks to establish chimeric equilibrium

(Figures 3H and S2C) and then separating the parabionts before subjecting them to either fasting or re-feeding. We tracked the GFP⁺Ly-6C^{hi} monocytes in partner mice. Despite the invasive surgical interventions, we detected notable differences in the location of GFP⁺Ly-6C^{hi} monocytes, finding considerably more monocytes in the blood and, conversely, fewer monocytes in the BM of re-fed mice (Figure 3I), yet again supporting the idea that re-feeding led to massive mobilization of sequestered cells.

The re-feeding data revealed a surge of rapidly mobilized monocytes back to the blood. We reasoned that the surge likely consisted of both newly generated monocytes that were trapped during fasting and of so-called returners—that is, mature circulating monocytes that returned to the BM via CXCR4 during fasting and that now were again released to the blood. We tested for hematopoiesis by measuring BrdU incorporation to hematopoietic stem and progenitor cells (HSPCs) and found a notable decrease in hematopoiesis during fasting that remained low 4 h after re-feeding (Figure S2D). We tested for the returners by enumerating monocytes under re-feeding conditions in mice with impaired re-mobilization: mice lacking CXCR4 (Figure 3J), the glucocorticoid receptor on monocytes (Figure 3K), and CRH in neurons of the PVH (Figure 3L). In all three cases, we did not see a surge of monocytes in blood after re-feeding, strongly suggesting that a major component of the surge consisted of “returners.”

The monocyte surge is dominated by aged Ly-6C^{hi} monocytes

The observation that the surge consisted of formerly circulating monocytes that had remobilized to the BM during fasting and then returned to the blood upon re-feeding raised a crucial question: were monocytes sequestered in the BM surviving longer than their circulating counterparts? By extension, was the re-feeding surge characterized by a chronologically older monocyte population? To begin testing these ideas, we implemented a double-pulse-chase strategy involving sequential injection of the nucleotide analogs EdU and BrdU (Figure 4A). Analysis of EdU and BrdU incorporation into medullary Ly-6C^{hi} monocytes revealed 4 populations (Figure 4B): the double negatives (BrdU⁻EdU⁻), representing cells that never had the opportunity to proliferate with either nucleotide analog present; the double positives (BrdU⁺EdU⁺), representing cells that proliferated once or more with both nucleotide analog present; and the single positives. Among the single positives, the EdU⁺BrdU⁻ monocytes (EdU monocytes henceforth) would have arisen prior to fasting, as this was when EdU was available before BrdU was injected. Conversely, the single positive EdU⁻BrdU⁺ monocytes (BrdU monocytes hereafter) would have arisen later, only after BrdU became available. Thus, we hypothesized that EdU monocytes were likely “old” (arisen pre-fast) whereas BrdU monocytes were “young” (i.e., arisen during fasting) monocytes.

With this in mind, we made several observations in the BM: first, EdU was similarly incorporated across the three groups (fed, fasted, fasted + re-fed) in HSPCs, indicating no major effects on progenitor proliferation, and thus no major effects on upstream hematopoiesis. BrdU incorporation was slightly reduced in certain HSPCs under fasting and fasting + re-feeding, which is in line with our prior finding of fasting suppressing hematopoiesis (Figures S3A, 3AB, and S2D). Second, while we found

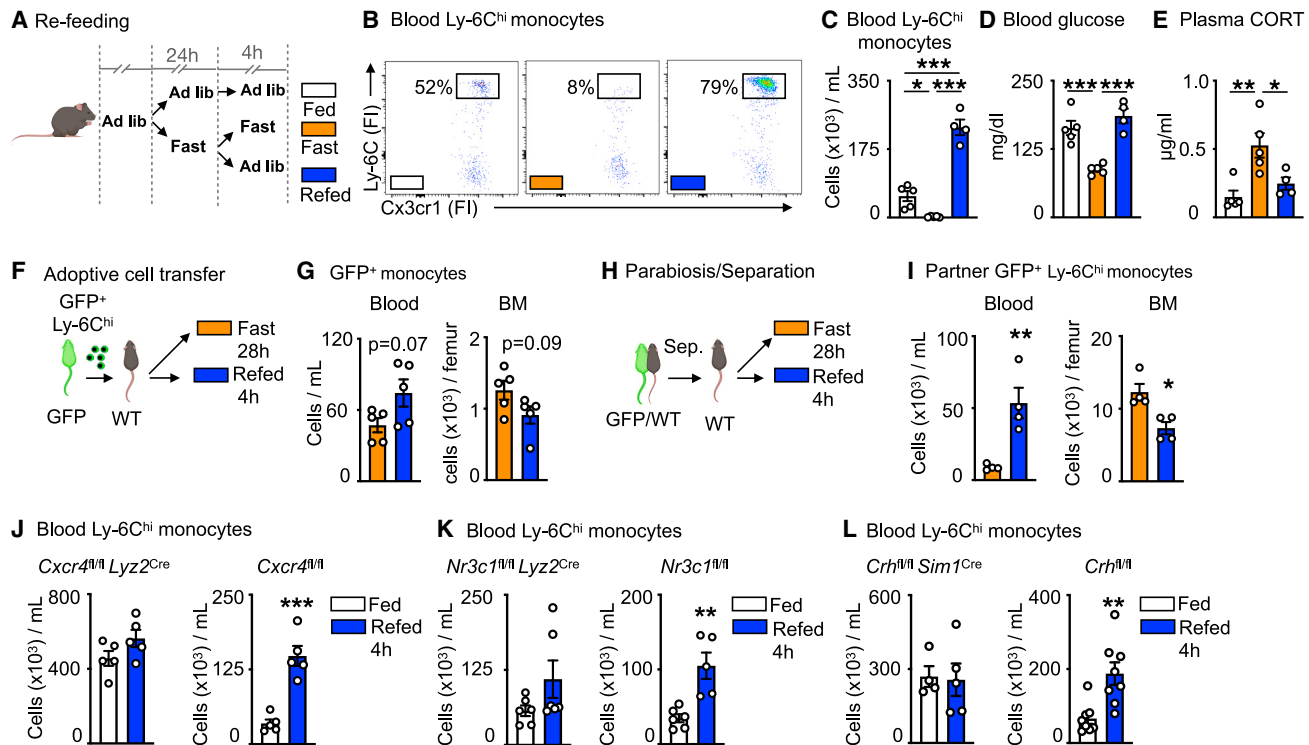


Figure 3. Re-feeding leads to a surge of monocytes into the bloodstream

(A) Mice were fasted for 24 h and divided into further fasting or re-feeding for 4 h. Control mice were fed *ad libitum*.
 (B) Representative flow-cytometry plots of blood Ly-6C^{hi} monocytes after feeding *ad libitum*, fasting for 28 h, or fasting for 24 h followed by 4 h of re-feeding. Ly-6C^{hi} monocytes are defined as CD45⁺ CD11b⁺ LIN1⁻ Ly-6G⁻ CX3CR1⁺ Ly-6C^{hi} (n = 4–5 per group).
 (C) Blood Ly-6C^{hi} monocytes after feeding *ad libitum*, fasting, or fasting + re-feeding (n = 4–5 per group; one-way ANOVA).
 (D) Blood-glucose concentration after feeding *ad libitum*, fasting, or fasting + re-feeding (n = 4–5 per group; one-way ANOVA).
 (E) Plasma corticosterone (CORT) concentration after feeding *ad libitum*, fasting, or fasting + re-feeding (n = 4–5 per group; one-way ANOVA).
 (F) Ly-6C^{hi} monocytes sorted from GFP-positive mice were injected intravenously into wild-type mice directly prior to submission to 28 h of fasting and 4 h of re-feeding.
 (G) Adoptively transferred monocytes in the blood and bone marrow (BM) of wild-type recipients. Adoptively transferred monocytes are defined as CD45⁺ GFP⁺. (n = 5 per group; unpaired t test.)
 (H) Parabiosis of GFP-positive and wild-type mice. After 2 weeks, mice were separated and wild-type mice were either fasted for 28 h or fasted for 24 h followed by 4 h of re-feeding.
 (I) GFP-positive Ly-6C^{hi} monocytes in the blood and BM of wild-type parabionts after fasting or fasting + re-feeding. (n = 4 per group; unpaired t test.)
 (J) Blood Ly-6C^{hi} monocytes in *Cxcr4*^{fl/fl} *Lyz2*^{Cre} and *Cxcr4*^{fl/fl} after feeding *ad libitum* or fasting + re-feeding. (n = 5 per group; unpaired t test.)
 (K) Blood Ly-6C^{hi} monocytes in *Nr3c1*^{fl/fl} *Lyz2*^{Cre} and *Nr3c1*^{fl/fl} after feeding *ad libitum* or fasting + re-feeding. (n = 5–6 per group; unpaired t test.)
 (L) Blood Ly-6C^{hi} monocytes in *Crh*^{fl/fl} *Sim1*^{Cre} and *Crh*^{fl/fl} after feeding *ad libitum* or fasting + re-feeding (n = 4–8 per group; unpaired t test). Data presented as mean ± SEM; *p < 0.05, **p < 0.01, ***p < 0.001. FI, fluorescence intensity; CORT, corticosterone; BM, bone marrow.
 See also [Figure S2](#).

a similar rate of relative EdU incorporation in monocytes in the BM, we found numerically more of these cells overall in the fasted and re-fed groups, compared with the *ad libitum*-fed mice (Figure 4C). Third, in line with previous findings, relative BrdU incorporation was lower in monocytes under fasting and fasting + re-feeding conditions, resulting in fewer BrdU monocytes in the BM of fasted and re-fed mice compared with *ad libitum*-fed mice (Figure 4C). These bone-marrow data suggested the persistence of chronologically old EdU monocytes in mice subjected to fasting along with reduced generation of chronologically “new” BrdU monocytes in those groups. In the blood, we likewise detected 4 monocyte populations (Figure 4D). Enumerating single EdU and single BrdU populations in the fed, fasted, and fasted + re-fed groups, we found that the surge during re-

feeding was dominated by EdU, rather than by BrdU monocytes (Figure 4E), thus indicating that the surge was dominated by old returners rather than newly produced cells. Together, these data provide evidence that the enlarged monocyte pool shortly after re-feeding consisted predominantly of older monocytes that had been sequestered in the BM during the fast (Figure 4F).

Fasting and re-feeding generates a chronologically older and transcriptionally distinct monocyte population

EdU and BrdU labeling revealed that the Ly-6C^{hi} monocyte surge into the bloodstream occurring 4 h after re-feeding largely consisted of cells produced prior to fasting. We sought to investigate if this pool was qualitatively different from *ad libitum*-fed conditions. We started by performing bulk RNA-seq of sorted blood

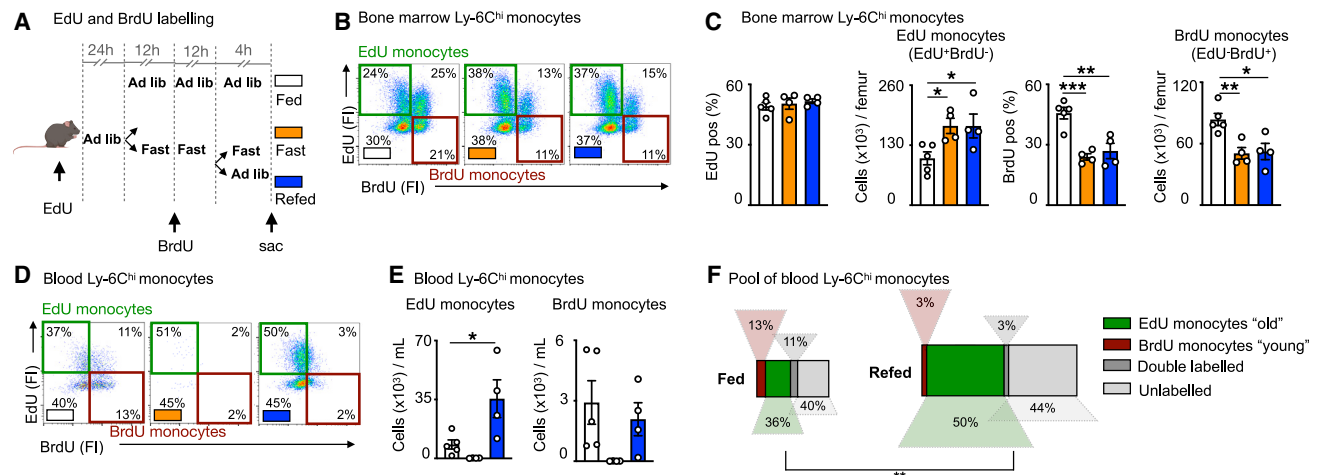


Figure 4. The monocyte surge is dominated by aged Ly-6C^{hi} monocytes

(A) EdU and BrdU were sequentially injected for labeling of Ly-6C^{hi} monocytes under feeding *ad libitum*, fasting, and fasting + re-feeding conditions. EdU was injected 24 h prior to fasting. BrdU was injected halfway through the fast. After a 24-h fast, fasted mice were divided into groups and were submitted to a further 4-h fast or 4 h of re-feeding.

(B) Representative flow-cytometry plots for Ly-6C^{hi} monocytes in the bone marrow under conditions of feeding *ad libitum*, fasting, and fasting + re-feeding. Ly-6C^{hi} monocytes are defined as CD45⁺ CD11b⁺ LIN1⁻ Ly-6G⁻ CX3CR1⁺ Ly-6C^{hi}. “EdU monocytes” are Ly-6C^{hi} monocytes with EdU-only label (labeled prior to fasting). “BrdU monocytes” are Ly-6C^{hi} monocytes with BrdU-only label (labeled under fasting). (n = 4–5 per group.)

(C) Relative EdU positivity of Ly-6C^{hi} monocytes and absolute EdU Ly-6C^{hi} monocyte count under feeding *ad libitum*, fasting, and fasting + re-feeding conditions in the bone marrow. Relative BrdU positivity of Ly-6C^{hi} monocytes and absolute BrdU Ly-6C^{hi} monocyte count under feeding *ad libitum*, fasting, and fasting + re-feeding conditions in the bone marrow. (n = 4–5 per group; one-way ANOVA.)

(D) Representative flow-cytometry plots for Ly-6C^{hi} monocytes in the blood under conditions of feeding *ad libitum*, fasting, and fasting + re-feeding. Ly-6C^{hi} monocytes are defined as CD45⁺ CD11b⁺ LIN1⁻ Ly-6G⁻ CX3CR1⁺ Ly-6C^{hi}. EdU monocytes are Ly-6C^{hi} monocytes with EdU-only label (labeled prior to fasting). BrdU monocytes are Ly-6C^{hi} monocytes with BrdU-only label (labeled under fasting). (n = 4–5 per group.)

(E) Absolute count of EdU monocytes and BrdU monocytes in the blood under feeding, fasting, or fasting + re-feeding conditions (n = 4–5 per group; one-way ANOVA).

(F) Relative quantification of Ly-6C^{hi} monocyte subpopulations, based on EdU and BrdU label in the blood after feeding or fasting + re-feeding conditions (n = 4–5 per group). The surface of the rectangle resembles the size of the whole pool of Ly-6C^{hi} monocytes in the blood. EdU monocytes can be considered chronologically older (old) than BrdU monocytes (young). (n = 4–5 per group; chi-square test. Data presented as mean ± SEM; *p < 0.05, **p < 0.01, ***p < 0.001. See also Figure S3.

Ly-6C^{hi} monocytes retrieved after fasting + re-feeding and feeding *ad libitum* (Figures 5A and S4A). As expected, RNA-expression differences overall were small, but 5 genes stood out as significantly and robustly differentially expressed after p value adjustment on genes prefiltered by absolute logFC > 1 (Figure 5B): *Ly-6i*, a member of the Ly-6 superfamily, expressed on immature monocytes²⁵ and *Tppp3* were decreased under fasting + re-feeding conditions, whereas *Lars2*, *Plppr3*, and *Chi3l3* (also known as *Ym1*), the latter of which is a known myeloid cell product and modulator^{26,27} were increased.

For more in-depth analysis, we performed single-cell RNA-seq on sorted blood Ly-6C^{hi} monocytes. We identified nine clusters, among which cluster 0, defined by *ApoE*, *Chi3l3*, and *Lpl* was considerably larger in the re-fed group (Figures 5C and 5D). Because bulk RNA-seq also revealed increased *Chi3l3* expression (Figures 5A and 5B), we measured *Chi3l3* in plasma, detecting higher protein concentrations during fasting (Figure 5E). As *Nr3c1^{fl/fl} Lyz2^{Cre}* mice did not augment *Chi3l3* during fasting (Figure 5E), we concluded that *Chi3l3* secretion under these conditions depended on glucocorticoid control of myeloid cells.

To acquire a more nuanced understanding of the temporal relationships between the monocyte clusters, we computed a trajectory graph from the uniform manifold approximation and projection (UMAP) dimensional space and ordered the cells in

pseudotime. According to the principal graph, clusters 3 and 4 were the most viable trajectory graph starting points. Cluster 3 was chosen as the more likely starting point because cluster 4 was enriched for Ly-6C intermediate marker genes (*Cd74*, *H2-Aa*, *H2-Eb1*, and *H2-Ab1*); Ly-6C^{hi} monocytes lose Ly-6C as they age and can convert to Ly-6C intermediate monocytes²⁸ (Figure 5F). Out of eight trajectories, three projected through or terminated at cluster 0, with trajectories falling later in pseudotime under fasting + re-feeding conditions (Figures 5G and S5B). Pseudotime analysis therefore supported our hypothesis that under fasting and subsequent re-feeding, older monocytes are released into the blood stream.

Fasting and re-feeding alters host response to infection

Having demonstrated that Ly-6C^{hi} monocytes released from the BM upon re-feeding are chronologically older and transcriptionally different, as well as larger in numbers, we wondered if the older pool would dominate a site of acute inflammation. To keep observations chronologically in line with our previous findings with the EdU and BrdU double-pulse-chase method, we tracked monocytes of fed and fasted mice in response to (lipopolysaccharide) LPS administered upon re-feeding (Figure 6A). After excluding Ly-6C^{hi} monocytes in the vasculature by intravenous CD45 labeling (Figure 6B), we found the expected four

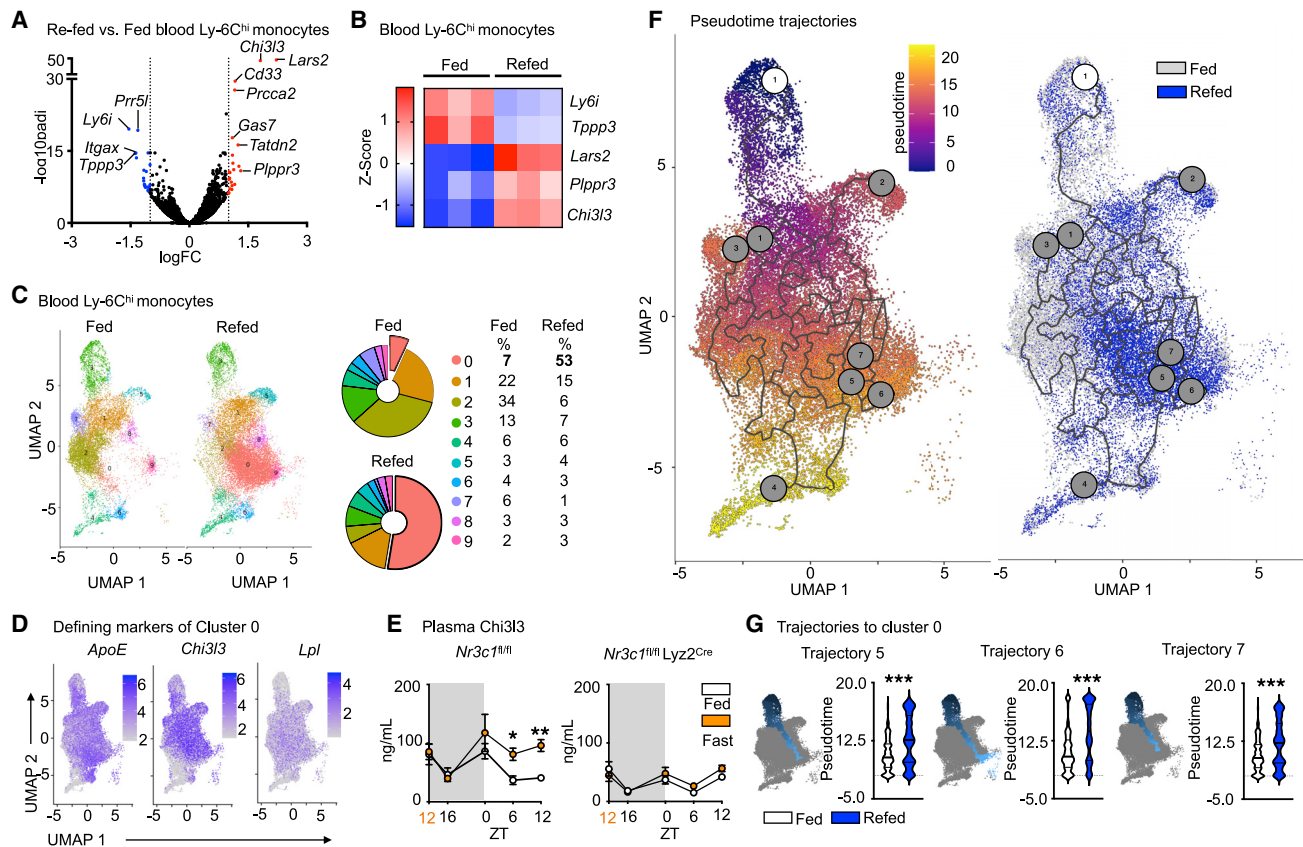


Figure 5. Fasting and re-feeding generates a chronologically older and transcriptionally distinct monocyte population

(A) Volcano plot indicating differentially regulated genes (FC > 1.0, FDR < 0.05, $p < 0.05$) of sorted blood Ly-6C^{hi} monocytes after feeding *ad libitum* or fasting for 24 h followed by 4 h re-feeding. ($n = 3$ per group, 4 mice pooled per sample).

(B) Heatmap of differentially expressed genes after conservative hierarchical clustering of sorted blood Ly-6C^{hi} monocytes after feeding *ad libitum* or fasting + re-feeding. ($n = 3$ samples per group, 4 mice pooled per sample).

(C) UMAP representations, colored by clusters computed by FindClusters function of Seurat and relative representation of the clusters of sorted blood Ly-6C^{hi} monocytes under fed and fasting + re-fed conditions. ($n = 1$ sample per group, 5 mice pooled per sample.)

(D) Expression of top 3 defining marker genes of cluster 0 visualized by feature plots.

(E) Plasma Chi3l3 in *Nr3c1^{fl/fl}* and *Nr3c1^{fl/fl} Lyz2^{Cre}* under feeding *ad libitum* or fasting conditions. Orange zeitgeber (ZT) indicates start of the fast ($n = 4-12$; time points are independent experiments; two-way ANOVA).

(F) Pseudotime computed with monocle 3. The white circled 1 indicates the root cell from where pseudotime analysis begins. Gray circles correspond to the different outcomes in the trajectory. UMAP representation overlaying conditions of feeding *ad libitum* and fasting + re-feeding.

(G) Pseudotime of trajectories 5, 6, and 7 projecting into cluster 0 in mice under feeding *ad libitum* and fasting + re-feeding. (Kolmogorov-Smirnov test. Data presented as mean \pm SEM; * $p < 0.05$, ** $p < 0.01$, *** $p < 0.001$.) ZT, zeitgeber. See also Figure S4.

populations in the lung parenchyma, including old EdU-positive and young BrdU-positive monocytes. Mice that had been fasted and re-fed along with LPS administration had a more pronounced monocyte recruitment to the lung, involving enhanced TNF α , and a larger contribution of old EdU monocytes compared with mice that were fed *ad libitum* (Figure 6C).

Because a 4-h re-feeding window gave mice enough time to normalize blood-glucose and CORT concentrations (Figures 3D and 3E), we next asked how long fasting + re-feeding monocytoysis would last. We noticed that the post-re-feeding surge persisted for at least 12 h before the system normalized itself by 24 h (Figure 6D). This return to monocytic homeostasis, at least numerically, lagged behind normalization of blood-glucose concentration (Figure 6E) and plasma CORT (Figure 6F) but correlated well with Chi3l3 plasma concentrations (Figure 6G),

consistent with the idea that Chi3l3 is a fasting-induced myeloid product. We therefore surmised that, even though repetitive fasting may have long-term consequences, acute effects on monocyte function within 1 day of fasting and re-feeding are also potentially meaningful. Pathway analysis from bulk RNA-seq revealed decreased activity of class-II antigen presentation, IFN β , and decreased innate immune signatures in monocytes of fasted + re-fed mice, suggesting that fasting + re-feeding may affect Ly-6C^{hi} monocytes' potential to respond to external challenges (Figures S5A, S5B, and S6).

Gram-negative bacteria, such as *Pseudomonas aeruginosa* (PAE) are a major cause of nosocomial pneumonia.²⁹ We infected mice intranasally with PAE after a 24-h fast followed by re-feeding for 4 h and tracked survival. Mice that underwent fasting + re-feeding died earlier and in larger numbers compared with *ad*

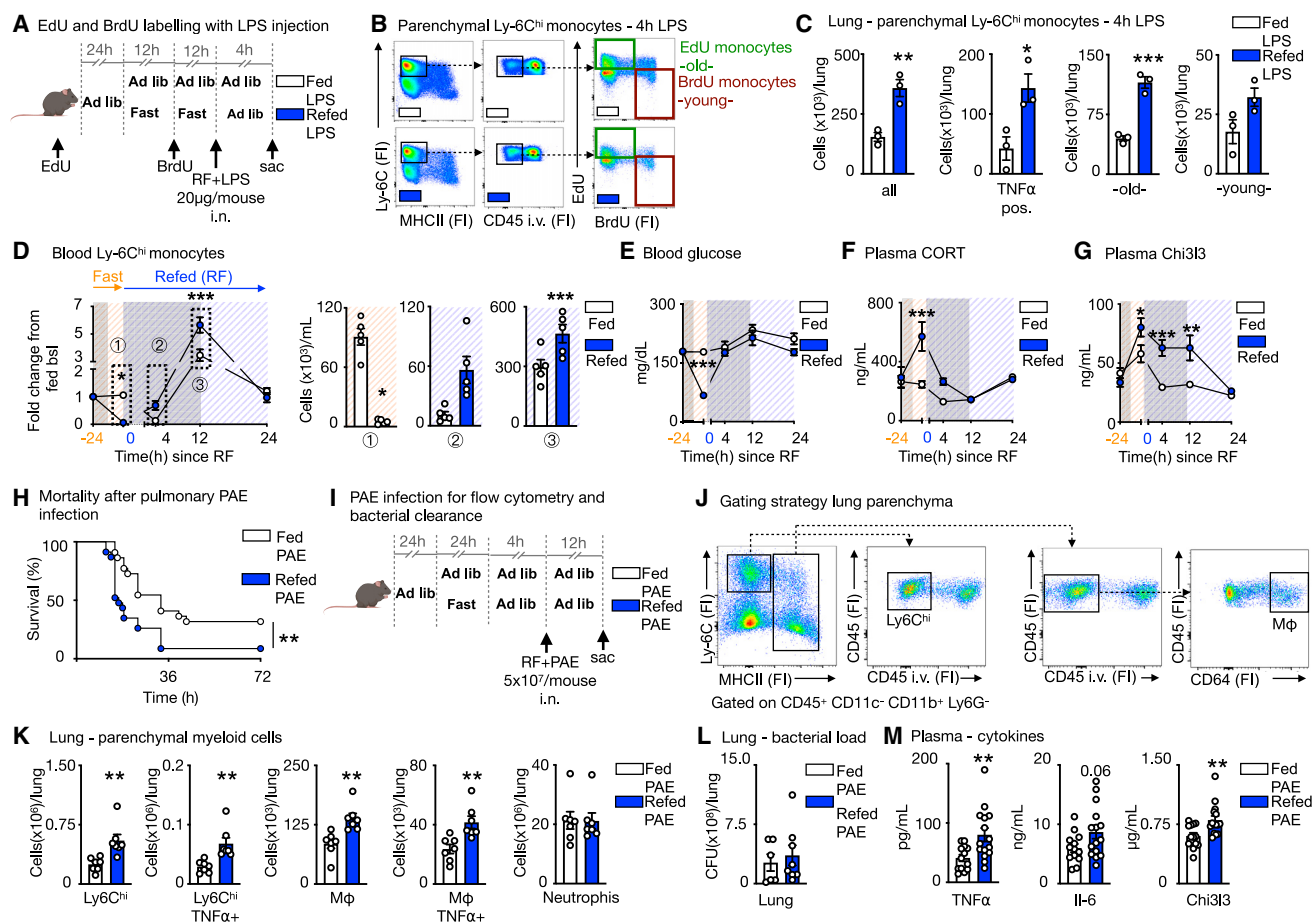


Figure 6. Fasting and re-feeding alters host response to infection

(A) EdU and BrdU were sequentially injected for labeling of Ly-6C^{hi} monocytes in mice under feeding *ad libitum* and fasting + re-feeding conditions. EdU was injected 24 h prior to fasting. BrdU was injected halfway through the fast. After a 24-h fast, fasted mice were re-fed for 4 h. LPS (20 µg/mouse) was administered intranasally at the time point of re-feeding and mice sacrificed 4 h later.

(B) Representative flow-cytometry plots for double labeling of Ly-6C^{hi} monocytes in the lung parenchyma. Intravascular Ly-6C^{hi} monocytes were excluded by intravenous CD45 staining prior to sacrifice. Ly-6C^{hi} monocytes are defined as CD45⁺ CD11b⁺ LIN1⁻ Ly-6G⁻ CX3CR1⁺ MHCII⁻ Ly-6C^{hi}. EdU monocytes are Ly-6C^{hi} monocytes with EdU-only label (labeled prior to fasting, old). BrdU monocytes are Ly-6C^{hi} monocytes with BrdU-only label (labeled under fasting, young). (n = 3 per group.)

(C) Absolute count of Ly-6C^{hi} monocytes and TNF α -positive Ly-6C^{hi} monocytes in the parenchyma after intranasal LPS challenge in mice undergoing feeding *ad libitum* or fasting + re-feeding. Absolute counts of old and young Ly-6C^{hi} monocytes in the parenchyma. Old are Ly-6C^{hi} monocytes with EdU-only label. Young are Ly-6C^{hi} monocytes with BrdU-only label (n = 3 per group; unpaired t test).

(D) Blood Ly-6C^{hi} monocytes under feeding or fasting + re-feeding conditions followed for 24 h after re-feeding normalized to group's baseline before fasting. Orange -24 h indicates baseline before start of a 24-h fast. Blue 0 indicates start of re-feeding. Bar graphs represent absolute Ly-6C^{hi} monocytes counts of indicated time points (n = 4-5 per group; time points are independent experiments; two-way ANOVA).

(E) Blood glucose under feeding or fasting + re-feeding conditions followed for 24 h after re-feeding. Orange -24 h indicates baseline before start of a 24-h fast. Blue 0 indicates start of re-feeding (n = 4-5 per group; time points are independent experiments; two-way ANOVA).

(F) Plasma corticosterone (CORT) under feeding or fasting + re-feeding conditions followed for 24 h after re-feeding. Orange -24 h indicates baseline before start of a 24-h fast. Blue 0 indicates start of re-feeding. (n = 4-5 per group; time points are independent experiments; two-way ANOVA.)

(G) Plasma Chi3I3 concentrations under feeding or fasting + re-feeding conditions followed for 24 h after re-feeding. Orange -24 h indicates baseline before start of a 24-h fast. Blue 0 indicates start of re-feeding. (n = 4-5 per group; time points are independent experiments; two-way ANOVA.)

(H) Mice were infected intranasally with *Pseudomonas aeruginosa* (PAE) at a dose of 5 × 10⁷/mouse. Re-fed mice were infected after a 24-h fast, followed by a 4-h re-feeding period. Control mice were fed *ad libitum* and both groups were followed for survival (n = 22-23 per group; two independent experiments combined; log-rank [Mantel-Cox] test).

(I) *Ad libitum*-fed mice and mice after 24-h fast followed by 4 h of re-feeding were intranasally infected with PAE at a dose of 5 × 10⁷/mouse and sacrificed 12 h after.

(J) To distinguish between circulating and parenchymal leukocytes, CD45 was injected intravenously before sacrifice. Representative gating strategy for flow cytometry on parenchymal Ly-6C^{hi} monocytes, defined as CD45⁺CD11c⁻CD11b⁺Ly6G⁻Ly-6C^{hi} MHCII⁻, and macrophages (M ϕ), defined as CD45⁺CD11c⁻CD11b⁺Ly6G⁻MHCII⁺CD64⁺ in the lung. (n = 7 per group.)

(K) Parenchymal myeloid cell content in the lung after infection with PAE as described in (I) (n = 7 per group; unpaired t test).

(legend continued on next page)

libitum-fed mice (Figure 6H). To correlate higher mortality with monocyte recruitment into the lung, we assessed myeloid cell content in the parenchyma 12 h after infection (Figures 6I and 6J). Fasting + re-feeding prior to infection with PAE led to higher content of Ly-6C^{hi} monocytes, and macrophages, as well as enhanced TNF α positivity, with no difference in neutrophil numbers (Figure 6K). Although we did not detect a difference in bacterial load in the lung (Figure 6L) or bronchoalveolar lavage (Figure S5C), we did observe more inflammation in the plasma, as assessed by higher circulating cytokine concentrations (Figure 6M). The monocytes were equally phagocytic (Figures S5D and S5E). These data suggest that the ensuing monocytic disequilibrium that occurs during prolonged fasting followed by re-feeding increases inflammation, thereby altering host response and leading to higher mortality compared with *ad libitum* feeding.

DISCUSSION

A key theme throughout this study is, arguably, the body's ability to limit energy expenditure during nutrient scarcity. Among leukocytes, monocytes are energetically costly if only because of their massive daily production in the BM. Unlike B and T cells, these circulating myeloid cells have a short half-life and thus rely on myelopoiesis for their replenishment. While the benefits of this phenomenon may be the availability of freshly made innate immune responders with finely tuned molecular machinery to meet the challenges of infection and injury, this study suggests that this process does seem to rely on an *ad libitum* supply of dietary energy. In the absence of such supply, the body slows down metabolic expenditure,^{30–32} limiting production and preserving—and thus extending—the lifespan of these already made, short-lived cells.

The BM as a hibernating tissue of choice for leukocytes has been explored before. Several recent studies have documented migration of leukocytes back to the marrow in response to environmental stimuli,^{13,14,17} although the consequence of such migration is poorly understood. As the birthplace of both red and white blood cells and the cradle of hematopoietic stem cells, the BM is, almost by definition, a privileged tissue tasked with ensuring that the blood pool remains refreshed throughout life. The reverse migration of monocytes during fasting described here raises a series of additional questions. First, it is not yet clear how monocytes survive in the BM during fasting. Perhaps the marrow produces its own energy to provide and nourish its resident cells during nutrient scarcity.³³ Or perhaps it simply shields sequestered monocytes from the harsh extramedullary environments that they would otherwise encounter in the circulation. Second, it remains to be seen whether a mechanistic link exists between the re-mobilization of circulating monocytes and the reduction of hematopoiesis during fasting. Are remobilized monocytes calibrating hematopoiesis, as aged neutrophils do,³⁴ or are these phenomena independent? Third, the mechanism orchestrating the return of monocytes to the circulation remains unclear and will need to be further studied. While it is likely

that the return of monocytes to the circulation coincides with lower CXCR4, it remains to be determined whether this is a passive consequence of less CORT or whether other, more active mechanisms contribute.

The role of the central nervous system in orchestrating large-scale leukocyte shifts documented here and elsewhere^{16,17,35} underscores the importance of focusing on brain-body communication in physiology and disease. While previous work indicated that hepatocyte-derived AMPK is responsible for shutting down monocyte mobilization,¹⁵ our study establishes the brain as the most upstream and consequential contributor. The series of signaling events that originate in the PVH and terminate at CORT release are known,^{36,37} but this study offers a perspective that merges fasting with the perception of hunger, stress, and complex changes in the leukocyte-distribution map. Heightened CORT itself, whether induced by extrinsic stressors or intrinsically by fasting, offers a potential explanation for altered host response via immunosuppressive mechanisms but is quickly normalized upon the removal of the stressor. Indeed, it may be monocytes staying “hangry” even after stress resolution that are key to the leukocytic reorganization and aggravated response in the periphery. Further inquiry will need to look deeper and more upstream, using synaptic retrograde tracing techniques, to better understand the links between metabolic sensing, the neurobiology of stress, and the efficiency of energetically costly hematopoiesis. Further work is also needed to better understand the implications of this work for human physiology. The concentration of plasma cortisol is expected to rise only after severe fasting in humans.³⁸ Thus, our data may be more relevant to conditions of more severe food scarcity or eating disorders where cortisol concentration is known to rise.³⁹

One of the interpretations of our data based on dual-pulse-chase tracking and pseudotime analyses of sequenced cells is that hibernating monocytes returning back to the blood upon re-feeding are chronologically older and transcriptionally distinct. The extent to which these transcriptional differences offer a glimpse of biological aging—as opposed to chronological aging, which is simply marked by the passage of time—is unclear, although we do note that the transcriptional differences are rather small. Nevertheless, the correlation between the preponderance of older monocytes, heightened inflammation, and altered functionality in response to infection, does suggest a disequilibrium, with an altered response of the monocyte population, perhaps evoking a few key features of biological aging. Regardless of how these cells are defined, there is a potential benefit to reducing the rate of hematopoiesis, whether by prolonged fasting,⁴⁰ exercising,⁴¹ better sleep hygiene^{16,42,43} or better diet.⁴⁴ Recent data suggest that accelerating the rate of leukocyte production precipitates clonal hematopoiesis, thus reducing hematopoietic diversity and conferring heightened risk of cardiovascular disease.^{42,43} It follows that measures aimed at reducing hematopoiesis may provide long-term benefit by virtue of preserving a diverse, nonclonal hematopoietic pool. Future studies will need to investigate these relationships in more mechanistic depth.

(L) Bacterial load after infection as described in (I) from homogenized lungs comparing fed and fasted + re-fed mice (n = 6–8 per group; unpaired t test).

(M) Plasma concentration of cytokines after infection as described in (I) (n = 13–15 per group; two experiments combined; unpaired t test. Data presented as mean \pm SEM; *p < 0.05, **p < 0.01, ***p < 0.001.) FI, fluorescence intensity; RF, re-feeding; PAE, *Pseudomonas aeruginosa*; M ϕ , macrophages. See also Figures S5 and S6.

In aggregate, our study provides a sequence of events occurring during fasting and re-feeding that link the HPA axis with monocytes and BM. Although fasting can protect against disease in numerous instances, our work argues there are limits, or at least a cost, to habits involving prolonged fasting and re-feeding. It is well documented that during starvation various bodily systems shut down or greatly diminish in a predictable sequence,⁴⁵ likely reflecting a hierarchy related to the survival imperative. In this context, continuous replenishment of circulating monocytes through myelopoiesis may be a type of luxury of plenty that is sacrificed relatively early even at a physiological cost.

Limitations of the study

Our study has limitations for translation into human physiology regarding the length of the fast and the related stress response. A 24-h fast in mice is different from fasting in humans, which makes our findings potentially more translatable to situations of severe food scarcity or eating disorders. We do not investigate mechanistically how monocytes are released back into circulation upon re-feeding but hypothesize that it is the result of re-established normalized plasma-CORT concentrations. Fasting + re-feeding led to detrimental outcomes in mice infected with *Pseudomonas aeruginosa*, which was chosen because it is a common strain for nosocomial pneumonia. We cannot exclude that other bacterial strains would have caused a different outcome.

STAR★METHODS

Detailed methods are provided in the online version of this paper and include the following:

- KEY RESOURCES TABLE
- RESOURCE AVAILABILITY
 - Lead contact
 - Materials availability
 - Data and code availability
- EXPERIMENTAL MODEL AND SUBJECT DETAILS
 - Mice
 - Bacteria
- METHOD DETAILS
 - Feeding and *fasting*
 - *In vitro* pHrodo™ assay
 - RNA extraction and cDNA
- QUANTIFICATION AND STATISTICAL ANALYSIS

SUPPLEMENTAL INFORMATION

Supplemental information can be found online at <https://doi.org/10.1016/j.immuni.2023.01.024>.

ACKNOWLEDGMENTS

This work was funded by the National Institutes of Health R35 HL135752, P01 HL131478, P01 HL142494 (to F.K.S.). H.J. was supported by the Deutsche Forschungsgemeinschaft (DFG, JA 2545/2-1). F.K. was supported by scholarships of the Deutsche Forschungsgemeinschaft (DFG, KA 4639/1-1) and the Deutsche Herzstiftung (S/03/19). L.H. was supported by Boehringer Ingelheim Fonds MD fellowship. C.S.M. was supported by NIH K99/R00 HL151750, R01 HL158534, and the Cure Alzheimer's Fund.

AUTHOR CONTRIBUTIONS

H.J., F.K., D.L., J.D., L.L.K., V.R., D.D., C.S.M., L.H., W.C.P., C.T.C., S.H., J.E.M., M.G.K., S.S., A.A., Y.I., and R.H.K. conducted experiments and collected and analyzed data. V.R., D.D., R.H.K., K.C., R.I.S., R.W., S.K.-S., and M.M. provided reagents and discussed results and strategy. H.J., F.K., D.L., J.D., L.L.K., V.R., D.D., S.K.-S., M.M., M.N., and F.K.S. designed experiments and interpreted data. H.J. and F.K. generated figures. F.K.S. supervised and directed the study and wrote the manuscript. All authors helped in editing the manuscript.

DECLARATION OF INTERESTS

M.N. has received funding or material research support from Alnylam, Biontronik, CSL Behring, GlycoMimetics, GSK, Medtronic, Novartis, and Pfizer as well as consulting fees from Lilly, Biogen, Gimv, IFM Therapeutics, Molecular Imaging, Sigilon, and Verseau Therapeutics. F.K.S. has received funds or material research support from Novartis, Partner Therapeutics, Pfizer, and Verseau Therapeutics.

INCLUSION AND DIVERSITY

We support inclusive, diverse, and equitable conduct of research.

Received: August 2, 2022

Revised: November 11, 2022

Accepted: January 19, 2023

Published: February 23, 2023

REFERENCES

1. Dehghan, M., Mente, A., Zhang, X., Swaminathan, S., Li, W., Mohan, V., Iqbal, R., Kumar, R., Wentzel-Viljoen, E., Rosengren, A., et al. (2017). Associations of fats and carbohydrate intake with cardiovascular disease and mortality in 18 countries from five continents (PURE): a prospective cohort study. *Lancet* **390**, 2050–2062.
2. Flegal, K.M., Kit, B.K., Orpana, H., and Graubard, B.I. (2013). Association of all-cause mortality with overweight and obesity using standard body mass index categories: a systematic review and meta-analysis. *JAMA* **309**, 71–82.
3. Yang, Q., Zhang, Z., Gregg, E.W., Flanders, W.D., Merritt, R., and Hu, F.B. (2014). Added sugar intake and cardiovascular diseases mortality among US adults. *JAMA Intern. Med.* **174**, 516–524.
4. Lumeng, C.N., and Saltiel, A.R. (2011). Inflammatory links between obesity and metabolic disease. *J. Clin. Invest.* **121**, 2111–2117.
5. Ma, T., Liaset, B., Hao, Q., Petersen, R.K., Fjære, E., Ngo, H.T., Lillefosse, H.H., Ringholm, S., Sonne, S.B., Treebak, J.T., et al. (2011). Sucrose counteracts the anti-inflammatory effect of fish oil in adipose tissue and increases obesity development in mice. *PLoS One* **6**, e21647.
6. Wilmut, E.G., Edwardson, C.L., Achana, F.A., Davies, M.J., Gorely, T., Gray, L.J., Khunti, K., Yates, T., and Biddle, S.J. (2012). Sedentary time in adults and the association with diabetes, cardiovascular disease and death: systematic review and meta-analysis. *Diabetologia* **55**, 2895–2905.
7. Papadimitriou-Olivgeris, M., Aretha, D., Zotou, A., Koutsileou, K., Zbouki, A., Lefkaditi, A., Sklavou, C., Marangos, M., and Fligou, F. (2016). The role of obesity in sepsis outcome among critically ill patients: A retrospective cohort analysis. *BioMed Res. Int.* **2016**, 5941279.
8. Brandhorst, S., and Longo, V.D. (2019). Dietary restrictions and nutrition in the prevention and treatment of cardiovascular disease. *Circ. Res.* **124**, 952–965.
9. Di Francesco, A., Di Germanio, C., Bernier, M., and de Cabo, R. (2018). A time to fast. *Science* **362**, 770–775.
10. Jensen, P., Christensen, R., Zachariae, C., Geiker, N.R., Schaadt, B.K., Stender, S., Hansen, P.R., Astrup, A., and Skov, L. (2016). Long-term effects of weight reduction on the severity of psoriasis in a cohort derived from a randomized trial: a prospective observational follow-up study. *Am. J. Clin. Nutr.* **104**, 259–265.

- Johnson, J.B., Summer, W., Cutler, R.G., Martin, B., Hyun, D.H., Dixit, V.D., Pearson, M., Nassar, M., Telljohann, R., Maudsley, S., et al. (2007). Alternate day calorie restriction improves clinical findings and reduces markers of oxidative stress and inflammation in overweight adults with moderate asthma. *Free Radic. Biol. Med.* **42**, 665–674.
- Shibolet, O., Alper, R., Avraham, Y., Berry, E.M., and Ilan, Y. (2002). Immunomodulation of experimental colitis via caloric restriction: role of Nk1.1+ T cells. *Clin. Immunol.* **105**, 48–56.
- Collins, N., Han, S.J., Enamorado, M., Link, V.M., Huang, B., Moseman, E.A., Kishton, R.J., Shannon, J.P., Dixit, D., Schwab, S.R., et al. (2019). The bone marrow protects and optimizes immunological memory during dietary restriction. *Cell* **178**, 1088–1101.e15.
- Nagai, M., Noguchi, R., Takahashi, D., Morikawa, T., Koshida, K., Komiyama, S., Ishihara, N., Yamada, T., Kawamura, Y.I., Muroi, K., et al. (2019). Fasting-refeeding impacts immune cell dynamics and mucosal immune responses. *Cell* **178**, 1072–1087.e14.
- Jordan, S., Tung, N., Casanova-Acebes, M., Chang, C., Cantoni, C., Zhang, D., Wirtz, T.H., Naik, S., Rose, S.A., Brocker, C.N., et al. (2019). Dietary intake regulates the circulating inflammatory monocyte pool. *Cell* **178**, 1102–1114.e17.
- McAlpine, C.S., Kiss, M.G., Rattik, S., He, S., Vassalli, A., Valet, C., Anzai, A., Chan, C.T., Mindur, J.E., Kahles, F., et al. (2019). Sleep modulates haematopoiesis and protects against atherosclerosis. *Nature* **566**, 383–387.
- Poller, W.C., Downey, J., Mooslechner, A.A., Khan, N., Li, L., Chan, C.T., McAlpine, C.S., Xu, C., Kahles, F., He, S., et al. (2022). Brain motor and fear circuits regulate leukocytes during acute stress. *Nature* **607**, 578–584.
- Pick, R., He, W., Chen, C.S., and Scheiermann, C. (2019). Time-of-day-dependent trafficking and function of leukocyte subsets. *Trends Immunol.* **40**, 524–537.
- Scheiermann, C., Kunisaki, Y., Lucas, D., Chow, A., Jang, J.E., Zhang, D., Hashimoto, D., Merad, M., and Frenette, P.S. (2012). Adrenergic nerves govern circadian leukocyte recruitment to tissues. *Immunity* **37**, 290–301.
- Wang, C., Lutes, L.K., Barnoud, C., and Scheiermann, C. (2022). The circadian immune system. *Sci. Immunol.* **7**, eabm2465.
- Yona, S., Kim, K.W., Wolf, Y., Mildner, A., Varol, D., Breker, M., Strauss-Ayali, D., Viukov, S., Guillemins, M., Misharin, A., et al. (2013). Fate mapping reveals origins and dynamics of monocytes and tissue macrophages under homeostasis. *Immunity* **38**, 79–91.
- Cain, D.W., Bortner, C.D., Diaz-Jimenez, D., Petrillo, M.G., Gruver-Yates, A., and Cidlowski, J.A. (2020). Murine glucocorticoid receptors orchestrate B cell migration selectively between bone marrow and blood. *J. Immunol.* **205**, 619–629.
- Barradas, M., Plaza, A., Colmenarejo, G., Lázaro, I., Costa-Machado, L.F., Martín-Hernández, R., Micó, V., López-Aceituno, J.L., Herranz, J., Pantoja, C., et al. (2022). Fatty acids homeostasis during fasting predicts protection from chemotherapy toxicity. *Nat. Commun.* **13**, 5677.
- Renquist, B.J., Murphy, J.G., Larson, E.A., Olsen, D., Klein, R.F., Ellacott, K.L., and Cone, R.D. (2012). Melanocortin-3 receptor regulates the normal fasting response. *Proc. Natl. Acad. Sci. USA* **109**, E1489–E1498.
- Pflugh, D.L., Maher, S.E., and Bothwell, A.L. (2000). Ly-6I, a new member of the murine Ly-6 superfamily with a distinct pattern of expression. *J. Immunol.* **165**, 313–321.
- Ikeda, N., Asano, K., Kikuchi, K., Uchida, Y., Ikegami, H., Takagi, R., Yotsumoto, S., Shibuya, T., Makino-Okamura, C., Fukuyama, H., et al. (2018). Emergence of immunoregulatory Ym1(+)Ly6C(hi) monocytes during recovery phase of tissue injury. *Sci. Immunol.* **3**, eaat0207.
- Shibuya, T., Kamiyama, A., Sawada, H., Kikuchi, K., Maruyama, M., Sawado, R., Ikeda, N., Asano, K., Kurotaki, D., Tamura, T., et al. (2021). Immunoregulatory monocyte subset promotes metastasis associated with therapeutic intervention for primary tumor. *Front. Immunol.* **12**, 663115.
- Mildner, A., et al. (2017). Genomic characterization of murine monocytes reveals C/EBPbeta transcription factor dependence of Ly6C(-) cells. *Immunity* **46**, 849–862.e7.
- Magill, S.S., Edwards, J.R., Bamberg, W., Beldavs, Z.G., Dumyati, G., Kainer, M.A., Lynfield, R., Maloney, M., McAllister-Hollod, L., Nadle, J., et al. (2014). Multistate point-prevalence survey of health care-associated infections. *N. Engl. J. Med.* **370**, 1198–1208.
- Buono, R., and Longo, V.D. (2018). Starvation, stress resistance, and cancer. *Trends Endocrinol. Metab.* **29**, 271–280.
- Longo, V.D., and Mattson, M.P. (2014). Fasting: molecular mechanisms and clinical applications. *Cell Metab.* **19**, 181–192.
- Nakamura, K., Nakamura, Y., and Kataoka, N. (2022). A hypothalamomedullary network for physiological responses to environmental stresses. *Nat. Rev. Neurosci.* **23**, 35–52.
- Devlin, M.J. (2011). Why does starvation make bones fat? *Am. J. Hum. Biol.* **23**, 577–585.
- Casanova-Acebes, M., Pitaval, C., Weiss, L.A., Nombela-Arrieta, C., Chèvre, R., A-González, N., Kunisaki, Y., Zhang, D., van Rooijen, N., Silberstein, L.E., et al. (2013). Rhythmic modulation of the hematopoietic niche through neutrophil clearance. *Cell* **153**, 1025–1035.
- Courties, G., Frodermann, V., Honold, L., Zheng, Y., Herisson, F., Schloss, M.J., Sun, Y., Presumey, J., Severe, N., Engblom, C., et al. (2019). Glucocorticoids regulate bone marrow B lymphopoiesis after stroke. *Circ. Res.* **124**, 1372–1385.
- Myers, M.G.J., and Olson, D.P. (2012). Central nervous system control of metabolism. *Nature* **491**, 357–363.
- Perry, R.J., Resch, J.M., Douglass, A.M., Madara, J.C., Rabin-Court, A., Kucukdereli, H., Wu, C., Song, J.D., Lowell, B.B., and Shulman, G.I. (2019). Leptin's hunger-suppressing effects are mediated by the hypothalamic-pituitary-adrenocortical axis in rodents. *Proc. Natl. Acad. Sci. USA* **116**, 13670–13679.
- Johnstone, A.M., Faber, P., Andrew, R., Gibney, E.R., Elia, M., Lobley, G., Stubbs, R.J., and Walker, B.R. (2004). Influence of short-term dietary weight loss on cortisol secretion and metabolism in obese men. *Eur. J. Endocrinol.* **150**, 185–194.
- Culbert, K.M., Racine, S.E., and Klump, K.L. (2016). Hormonal factors and disturbances in eating disorders. *Curr. Psychiatry Rep.* **18**, 65.
- Cheng, C.W., Adams, G.B., Perin, L., Wei, M., Zhou, X., Lam, B.S., Da Sacco, S., Mirisola, M., Quinn, D.I., Dorff, T.B., et al. (2014). Prolonged fasting reduces IGF-1/PKA to promote hematopoietic-stem-cell-based regeneration and reverse immunosuppression. *Cell Stem Cell* **14**, 810–823.
- Frodermann, V., Rohde, D., Courties, G., Severe, N., Schloss, M.J., Amatullah, H., McAlpine, C.S., Cremer, S., Hoyer, F.F., Ji, F., et al. (2019). Exercise reduces inflammatory cell production and cardiovascular inflammation via instruction of hematopoietic progenitor cells. *Nat. Med.* **25**, 1761–1771.
- Heyde, A., Rohde, D., McAlpine, C.S., Zhang, S., Hoyer, F.F., Gerold, J.M., Cheek, D., Iwamoto, Y., Schloss, M.J., Vandoorne, K., et al. (2021). Increased stem cell proliferation in atherosclerosis accelerates clonal hematopoiesis. *Cell* **184**, 1348–1361.e22.
- McAlpine, C.S., Kiss, M.G., Zuraikat, F.M., Cheek, D., Schirolli, G., Amatullah, H., Huynh, P., Bhatti, M.Z., Wong, L.P., Yates, A.G., et al. (2022). Sleep exerts lasting effects on hematopoietic stem cell function and diversity. *J. Exp. Med.* **219**.
- Bhattacharya, R., Zekavat, S.M., Uddin, M.M., Pirruccello, J., Niroula, A., Gibson, C., Griffin, G.K., Libby, P., Ebert, B.L., Bick, A., et al. (2021). Association of diet quality with prevalence of clonal hematopoiesis and adverse cardiovascular events. *JAMA Cardiol.* **6**, 1069–1077.
- Cahill, G.F.J. (1970). Starvation in man. *N. Engl. J. Med.* **282**, 668–675.
- Robbins, C.S., Hilgendorf, I., Weber, G.F., Theurl, I., Iwamoto, Y., Figueiredo, J.L., Gorbатов, R., Sukhova, G.K., Gerhardt, L.M., Smyth, D., et al. (2013). Local proliferation dominates lesional macrophage accumulation in atherosclerosis. *Nat. Med.* **19**, 1166–1172.
- Ewels, P.A., Peltzer, A., Fillinger, S., Patel, H., Alneberg, J., Wilm, A., Garcia, M.U., Di Tommaso, P., and Nahnsen, S. (2020). The nf-core

- framework for community-curated bioinformatics pipelines. *Nat. Biotechnol.* **38**, 276–278.
48. Ewels, P., Magnusson, M., Lundin, S., and Källér, M. (2016). MultiQC: summarize analysis results for multiple tools and samples in a single report. *Bioinformatics* **32**, 3047–3048.
 49. Dobin, A., Davis, C.A., Schlesinger, F., Drenkow, J., Zaleski, C., Jha, S., Batut, P., Chaisson, M., and Gingeras, T.R. (2013). STAR: ultrafast universal RNA-seq aligner. *Bioinformatics* **29**, 15–21.
 50. Patro, R., Duggal, G., Love, M.I., Irizarry, R.A., and Kingsford, C. (2017). Salmon provides fast and bias-aware quantification of transcript expression. *Nat. Methods* **14**, 417–419.
 51. Love, M.I., Huber, W., and Anders, S. (2014). Moderated estimation of fold change and dispersion for RNA-seq data with DESeq2. *Genome Biol.* **15**, 550.
 52. Wu, T., Hu, E., Xu, S., Chen, M., Guo, P., Dai, Z., Feng, T., Zhou, L., Tang, W., Zhan, L., et al. (2021). clusterProfiler 4.0: A universal enrichment tool for interpreting omics data. *Innovation (Camb)* **2**, 100141.
 53. Subramanian, A., Tamayo, P., Mootha, V.K., Mukherjee, S., Ebert, B.L., Gillette, M.A., Paulovich, A., Pomeroy, S.L., Golub, T.R., Lander, E.S., et al. (2005). Gene set enrichment analysis: a knowledge-based approach for interpreting genome-wide expression profiles. *Proc. Natl. Acad. Sci. USA* **102**, 15545–15550.
 54. Hao, Y., Hao, S., Andersen-Nissen, E., Mauck, W.M., Zheng, S., Butler, A., Lee, M.J., Wilk, A.J., Darby, C., Zager, M., et al. (2021). Integrated analysis of multimodal single-cell data. *Cell* **184**, 3573–3587.e29.
 55. Qiu, X., Mao, Q., Tang, Y., Wang, L., Chawla, R., Pliner, H.A., and Trapnell, C. (2017). Reversed graph embedding resolves complex single-cell trajectories. *Nat. Methods* **14**, 979–982.

STAR★METHODS

KEY RESOURCES TABLE

REAGENT or RESOURCE	SOURCE	IDENTIFIER
Antibodies		
Brilliant Violet 711™ anti-mouse CD45 clone 30-F11	BioLegend	Cat# 103147
PE anti-mouse CD45.1 clone A20	BioLegend	Cat# 110707
PE/Cyanine7 anti-mouse CD45.2 clone 104	BioLegend	Cat# 109829
PE anti-mouse CD3 clone 17A2	BioLegend	Cat# 100206
PE anti-mouse CD90.2 clone 3O-H12	BioLegend	Cat# 105308
PE anti-mouse CD19 clone 6D5	BioLegend	Cat# 115508
PE anti-mouse B220 clone RA3-6B2	BD Biosciences	Cat# 553089
PE anti-mouse NK-1.1 clone PK136	BioLegend	Cat# 108708
APC anti-mouse Ly-6G clone 1A8	BioLegend	Cat# 127614
FITC anti-mouse Ly-6C clone HK1.4	BioLegend	Cat# 128006
Alexa Fluor® 700 anti-mouse I-A/I-E clone M5/114.15.2	BioLegend	Cat# 107602
APC/Fire™ 810 anti-mouse F4/80 clone BM8	BioLegend	Cat# 123166
APC/Cyanine7 anti-mouse/human CD11b clone M1/70	BioLegend	Cat# 101226
Brilliant Violet 605™ anti-mouse CD115 clone AFS98	BioLegend	Cat# 135517
PE anti-mouse TER-119 clone TER-119	BioLegend	Cat# 116208
FITC anti-mouse CD34 clone RAM34	ThermoFisher	Cat# 11-0341-85
APC anti-mouse CD11c clone N418	BioLegend	Cat# 117310
PE anti-mouse CD127 clone SB/199	BioLegend	Cat# 121112
PerCP/Cyanine5.5 anti-mouse CD16/32 clone 93	BioLegend	Cat# 101324
PerCP/Cyanine5.5 anti-mouse CD150	BioLegend	Cat# 115922
APC anti-mouse CD135 clone A2F10	BioLegend	Cat# 135310
Alexa Fluor® 700 anti-mouse CD48 clone HM48-1	BioLegend	Cat# 103426
PE/Cyanine7 anti-mouse CD117 (c-Kit) clone 2B8	BioLegend	Cat# 105814
APC/Cyanine7 anti-mouse Ly-6A/E (Sca-1) clone D7	BioLegend	Cat# 108126
APC anti-mouse CD8a clone 53-6.7	BD Biosciences	Cat# 553035
Pacific Blue™ anti-mouse CD4 clone GK1.5	BioLegend	Cat# 100428
PE anti-mouse Siglec-F clone E50-2440	BD Biosciences	Cat# 562068
PE anti-mouse CXCR4 clone 2B11	ThermoFisher	Cat# 12-9991-82
PE/Cyanine7 anti-mouse CX3CR1 clone SA011F11	BioLegend	Cat# 149016
PE/Cyanine7 anti-mouse TNF- α clone MP6-XT22	BioLegend	Cat# 506324
PE/Dazzle™ 594 anti-mouse CD64 clone X54-5/7.1	BioLegend	Cat# 139320
AF647™ anti-BrdU clone MoBU-1	ThermoFisher	Cat# B35133
Brilliant Violet 650™ anti-mouse CD192 (CCR2)	BioLegend	Cat# 150613
Bacterial and virus strains		
<i>Pseudomonas aeruginosa</i> , Strain Boston 41501	ATCC	ATCC# 27853
Chemicals, peptides, and recombinant proteins		
Corticosterone: HBC complex	Sigma-Aldrich	Cat# C174
pHrodo™ Red Phagocytosis Particle Labeling Kit for Flow Cytometry	Thermo Fisher	Cat# A10026
pHrodo™ Red <i>E. coli</i> BioParticles™ Conjugate for Phagocytosis	Thermo Fisher	Cat# P35361
Critical commercial assays		
RNeasy Mini Kit	Qiagen	Cat# 74104
High-Capacity cDNA Reverse Transcription Kit	Thermo Fisher	Cat# 4368814

(Continued on next page)

Continued

REAGENT or RESOURCE	SOURCE	IDENTIFIER
Corticosterone ELISA kit	Abcam	Cat# ab108821
Mouse YM1/Chitinase3-like 3 DuoSet ELISA	R&D Systems	Cat# DY2446
Mouse IL-6 Quantikine ELISA Kit	R&D Systems	Cat# M6000B
Mouse TNF-alpha Quantikine ELISA Kit	R&D Systems	Cat# MTA00B
Free Fatty Acid Quantitation Kit	Sigma-Aldrich	Cat# MAK044
Click-iT™ Plus EdU Pacific Blue™	Thermo Fisher	Cat# C10636
Flow Cytometry Assay Kit		

Deposited data

Single cell RNA sequencing data	Gene Expression Omnibus	GSE217597
Bulk RNA sequencing data	Gene Expression Omnibus	GSE217597

Experimental models: Organisms/strains

C57BL/6J	The Jackson Laboratory	Strain 000664
C57BL/6-Tg(UBC-GFP)30Scha/J	The Jackson Laboratory	Strain 004353
B6.129P2-Lyz2tm1(cre)lfo/J	The Jackson Laboratory	Strain 004781
B6.129P2-Cxcr4tm2Yzo/J	The Jackson Laboratory	Strain 008767
B6.Cg-Nr3c1tm1.1Jda/J	The Jackson Laboratory	Strain 021021
STOCK Prkaa1tm1.1Sjm/J	The Jackson Laboratory	Strain 014141
B6.129S4(Cg)-Arntl1tm1Weit/J	The Jackson Laboratory	Strain 007668
STOCK Slc2a1tm1.1Stma/AbelJ	The Jackson Laboratory	Strain 031871
B6.FVB(129X1)-Tg(Sim1Cre)1Low/J	The Jackson Laboratory	Strain 006451
B6.129S4(Cg)-Crhm2.1Maj/J	The Jackson Laboratory	Strain 030110
B6.129S4-Ccr2tm1lfc/J	The Jackson Laboratory	Strain 004999
C.129S7(B6)-Itgb2tm2Bay/AbhmJ	The Jackson Laboratory	Strain 027003
B6.129P2(Cg)-Cx3cr1tm1Litt/J	The Jackson Laboratory	Strain 005582
B6.129S7-Rag1tm1Mom/J	The Jackson Laboratory	Strain 002216
BALB/cJ	The Jackson Laboratory	Strain 000651

Oligonucleotides

Mouse GAPD Mm99999915_g1	Thermo Fisher	Cat# 4331182
Mouse ACTB Mm00607939_s1	Thermo Fisher	Cat# 4331182
Mouse Clock Mm00455950_m1	Thermo Fisher	Cat# 4331182
Mouse Arntl Mm00500226_m1	Thermo Fisher	Cat# 4331182
Mouse Nr1d2 Mm01310356_g1	Thermo Fisher	Cat# 4331182
Mouse Per1 Mm00501813_m1	Thermo Fisher	Cat# 4331182
Mouse Cry1 Mm00514392_m1	Thermo Fisher	Cat# 4331182
Mouse Selp1g Mm01204601_m1	Thermo Fisher	Cat# 4331182
Mouse Cd44 Mm01277161_m1	Thermo Fisher	Cat# 4331182
Mouse Itgal Mm00801807_m1	Thermo Fisher	Cat# 4331182
Mouse Itgam Mm00434455_m1	Thermo Fisher	Cat# 4331182
Mouse Itgb1 Mm01253230_m1	Thermo Fisher	Cat# 4331182
Mouse Itgb2 Mm00434513_m1	Thermo Fisher	Cat# 4331182
Mouse Itga4 Mm01277951_m1	Thermo Fisher	Cat# 4331182
Mouse Itga5 Mm00439797_m1	Thermo Fisher	Cat# 4331182
Mouse Itga6 Mm00434375_m1	Thermo Fisher	Cat# 4331182
Mouse Ccr1 Mm00438260_s1	Thermo Fisher	Cat# 4331182
Mouse Cxcr3 Mm9999054_s1	Thermo Fisher	Cat# 4331182
Mouse Cxcr4 Mm01996749_s1	Thermo Fisher	Cat# 4331182
Mouse Cx3cr1 Mm02620111_s1	Thermo Fisher	Cat# 4331182
Mouse Ilb1 Mm00434228_m1	Thermo Fisher	Cat# 4331182

(Continued on next page)

Continued

REAGENT or RESOURCE	SOURCE	IDENTIFIER
Mouse Tnf Mm00443258_m1	Thermo Fisher	Cat# 4331182
Mouse Ccr2 Mm99999051_gH	Thermo Fisher	Cat# 4331182
Software and algorithms		
FlowJo v10	FlowJo	https://www.flowjo.com/
GraphPad Prism v9	GraphPad Software	https://www.graphpad.com/
BioRender	BioRender	https://biorender.com
R Differential gene expression analysis		
R version 4.2.1, Platform: aarch64-apple-darwin20 (64-bit); OS: macOS Monterey 12.6.1	aarch64-apple-darwin20 (64-bit)	N/A
scales_1.2.1	CRAN/BiocManager	N/A
clusterProfiler_4.6.0	CRAN/BiocManager	N/A
tidyr_1.2.1	CRAN/BiocManager	N/A
dplyr_1.0.10	CRAN/BiocManager	N/A
ggplot2_3.3.6	CRAN/BiocManager	N/A
GenomicRanges_1.50.0	CRAN/BiocManager	N/A
MatrixGenerics_1.10.0	CRAN/BiocManager	N/A
ggthemes_4.2.4	CRAN/BiocManager	N/A
org.Hs.eg.db_3.16.0	CRAN/BiocManager	N/A
immunarch_0.8.0	CRAN/BiocManager	N/A
EnhancedVolcano_1.16.0	CRAN/BiocManager	N/A
genefilter_1.80.0	CRAN/BiocManager	N/A
GenomeInfoDb_1.34.0	CRAN/BiocManager	N/A
matrixStats_0.62.0	CRAN/BiocManager	N/A
msigdb_7.5.1	CRAN/BiocManager	N/A
org.Mm.eg.db_3.16.0	CRAN/BiocManager	N/A
patchwork_1.1.2	CRAN/BiocManager	N/A
ggrepel_0.9.1	CRAN/BiocManager	N/A
DESeq2_1.38.0	CRAN/BiocManager	N/A
IRanges_2.32.0	CRAN/BiocManager	N/A
glmPCA_0.2.0	CRAN/BiocManager	N/A
pathview_1.38.0	CRAN/BiocManager	N/A
AnnotationDbi_1.60.0	CRAN/BiocManager	N/A
data.table_1.14.4	CRAN/BiocManager	N/A
glmGamPoi_1.10.0	CRAN/BiocManager	N/A
SummarizedExperiment_1.28.0	CRAN/BiocManager	N/A
S4Vectors_0.36.0	CRAN/BiocManager	N/A
RColorBrewer_1.1-3	CRAN/BiocManager	N/A
enrichplot_1.18.0	CRAN/BiocManager	N/A
gridExtra_2.3	CRAN/BiocManager	N/A
dtplyr_1.2.2	CRAN/BiocManager	N/A
ggbeeswarm_0.6.0	CRAN/BiocManager	N/A
Biobase_2.58.0	CRAN/BiocManager	N/A
BiocGenerics_0.44.0	CRAN/BiocManager	N/A
pheatmap_1.0.12	CRAN/BiocManager	N/A
R scRNA analysis		
monocle3_1.2.9	GitHub	N/A
IRanges_2.32.0	CRAN/BiocManager	N/A
BiocGenerics_0.44.0	CRAN/BiocManager	N/A

(Continued on next page)

Continued

REAGENT or RESOURCE	SOURCE	IDENTIFIER
SeuratObject_4.1.2	GitHub	N/A
SingleCellExperiment_1.20.0	CRAN/BiocManager	N/A
S4Vectors_0.36.0	CRAN/BiocManager	N/A
SeuratDisk_0.0.0.9020	GitHub	N/A
Seurat_4.2.0	GitHub	N/A
SummarizedExperiment_1.28.0	CRAN/BiocManager	N/A
MatrixGenerics_1.10.0	GitHub	N/A
SeuratWrappers_0.3.1	GitHub	N/A
magrittr_2.0.3	CRAN/BiocManager	N/A
GenomicRanges_1.50.0	CRAN/BiocManager	N/A
matrixStats_0.62.0	CRAN/BiocManager	N/A
SeuratData_0.2.2	GitHub	N/A
patchwork_1.1.2	CRAN/BiocManager	N/A
GenomeInfoDb_1.34.0	CRAN/BiocManager	N/A
Biobase_2.58.0	CRAN/BiocManager	N/A
sp_1.5-0	CRAN/BiocManager	N/A
ggplot2_3.3.6	CRAN/BiocManager	N/A

RESOURCE AVAILABILITY

Lead contact

Further information and requests for resources and reagents should be directed to and will be fulfilled by the lead contact, Filip K. Swirski (filip.swirski@mssm.edu).

Materials availability

This study did not generate unique reagents.

Data and code availability

- Single-cell RNA-seq data have been deposited at GEO and are publicly available as of the date of publication. Accession numbers are listed in the [key resources table](#).
- Any additional information required to reanalyze the data reported in this paper is available from the [lead contact](#) upon request.

EXPERIMENTAL MODEL AND SUBJECT DETAILS

Mice

C57BL/6J, C57BL/6-Tg(UBC-GFP)30Scha/J (GFP-UBI), B6.129P2-Lyz2^{tm1(cre)lfc}/J (Lyz2^{Cre}), B6.129P2-Cxcr4^{tm2Yzo}/J (Cxcr4^{fl/fl}), B6.Cg-Nr3c1^{tm1.1Jda}/J (Nr3c1^{fl/fl}), STOCK Prkaa1^{tm1.1Sjm}/J (Prkaa1^{fl/fl}), B6.129S4(Cg)-Arnt^{tm1Weit}/J (Arnt^{fl/fl}), STOCK Slc2a1^{tm1.1Stma}/AbelJ (Slc2a1^{fl/fl}), B6.FVB(129X1)-Tg(Sim1Cre)1Lowl/J (Sim1^{Cre}), B6.129S4(Cg)-Crh^{tm2.1Maj}/J (Crh^{fl/fl}), B6.129S4-Ccr2^{tm1lfc}/J (Ccr2^{-/-}), C.129S7(B6)-Itgb2^{tm2Bay}/AbhmJ (Cd18^{-/-}), B6.129P2(Cg)-Cx3cr1^{tm1Litt}/J (Cx3cr1^{ΔGFP/GFP}), B6.129S7-Fag1^{tm1Mom}/J (Fag1^{-/-}), and BALB/cJ were purchased from The Jackson Laboratory. Genotyping for each strain was performed as recommended on The Jackson Laboratory website. Relevant mice were crossed to generate Cxcr4^{fl/fl} Lyz2^{Cre}, Nr3c1^{fl/fl} Lyz2^{Cre}, Crh^{fl/fl} Sim1^{Cre}, Prkaa1^{fl/fl} Lyz2^{Cre}, Arnt^{fl/fl} Lyz2^{Cre}, Slc2a1^{fl/fl} Lyz2^{Cre} and respective litter mate controls. All experiments were performed on male and female 7 week- to 1 year-old mice with age- and sex-matched controls. All mice were housed on a 12h/12h light/dark cycle at 22°C with unrestricted access to food and water. Where appropriate, mice were randomly assigned to groups and experiments were performed blinded. All protocols were approved by the Animal Review Committee at the Massachusetts General Hospital (protocols 2011N000035 and 2015N000044) and/or the Animal Review Committee at the Mount Sinai Hospital (PROTO202000262 and PROTO20220000111) and complied with all relevant ethical regulations.

Bacteria

The ATCC 27853 strain *Pseudomonas aeruginosa* was grown overnight on tryptic soy agar plates at 37°C. Single colonies were picked and grown overnight in tryptic soy broth at 37°C with constant shaking.

METHOD DETAILS

Feeding and fasting

Mice were single- or group-housed on a 12:12-h light-dark cycle at 22°C with free access to chow diet and water. Under fasting conditions, mice were fasted for periods up to 28 hours starting at ZT12 with unlimited access to water. Fed controls had food available ad libitum.

Re-feeding

After a 24h fast, chow diet was put back into the cage, mice were allowed to eat ad libitum.

Platelet depletion

36h prior to fasting, mice were i.p. injected with anti-GP1BA/ CD42b antibodies or isotope control to deplete platelets.

Cell sorting

Blood, spleen or/and bone marrow cell suspensions were stained to identify the indicated cell populations and cells were sorted on a FACS Aria II cell sorter (BD Biosciences) directly into either RLT buffer for subsequent RNA isolation or collecting medium.

Adoptive transfer

An equal amount of sorted Ly-6C^{hi} monocytes from GFP-UBI mice was injected into the retrobulbar plexus directly before initiation of fasting.

Parabiosis

The procedure, adapted from was conducted as previously described.⁴⁶ Briefly, after shaving the corresponding lateral aspects of a GFP-UBI and a wild type mouse, matching skin incisions were made from behind the ear to the tail of each mouse, and the subcutaneous fascia was bluntly dissected to create about 0.5 cm of free skin. The scapulas were sutured using a mono-nylon 5.0 (Ethicon, Albuquerque, NM), and the dorsal and ventral skins were approximated by continuous suture. Mice were joined for 2 weeks. After, mice in parabiosis were surgically separated by a reversal of the procedure. Percent chimerism in the blood was defined for gated Ly-6C^{hi} monocytes as %GFP+ (%GFP⁺ & %GFP⁻)⁻¹ in wild type mice. Mice in the fasting group were fasted directly after separation for 28 hrs and mice in the refed group refed after 24h for 4h.

Intravital microscopy

Fed mice versus fasted mice were anesthetized with 1-3% isoflurane and 2 l/min oxygen anesthesia for monocyte imaging. Mice were kept on a 37°C heating plate during the whole procedure. Fluorescent agents, FITC dextran (2 million Da) for labelling the vasculature and PE-labeled anti-CD115 antibodies to visualize Ly-6C^{hi} monocytes (5 μl antibody stock in 50 μl PBS), were injected i.v. The femoral vein was exposed on a 37°C heated plate and the vessel lumen was imaged confocally. The entire surgical and imaging procedure was kept to a maximum of 1h. Imaging was done with an Olympus XLUMPLFLN 20X W NA:1.00 water immersion objective on an Olympus custom made confocal multi-photon microscope using 473 nm and 559 nm diode-lasers with a DM405/473/559 dichroic mirror, a SDM560 beam splitter, and BA490-540 and BA575-675 emission filters (Olympus America Inc.).

Adrenalectomy

Both adrenal glands were surgically removed via bilateral dorso-lateral subcostal access routes. Sham-operated mice served as controls. Post surgery, adrenalectomized mice received saline as drinking water. Mice were allowed to recover for >7 d before further manipulation.

Corticosterone injections

Mice were intraperitoneally injected with either vehicle (PBS) or corticosterone (5 mg/kg bodyweight, Corticosterone: HBC complex, Sigma-Aldrich, C174) under short isoflurane anaesthesia. Blood was withdrawn and analyzed 1 h after injection.

EdU and BrdU incorporation

To assess cell proliferation, 1 mg BrdU was injected intraperitoneally 2 h before euthanasia. For cell labelling assays, 1 mg BrdU and 250 μg EdU were injected intraperitoneally at indicated time points. BrdU-positive cells were stained with a BrdU flow kit (BD Biosciences) and EdU-positive cells with a Click-iT™ Plus EdU Flow Cytometry assay kit (Thermo Fisher)

pHrodo™ labeling of *Pseudomonas aeruginosa* particles

Pseudomonas aeruginosa particles were labeled based on the manufacturers' instructions of the pHrodo™ Red Phagocytosis Particle Labeling Kit for Flow Cytometry (Thermo Fisher, A10026).

LPS inoculation

Mice were anesthetized with isoflurane and intranasally infected with 20μg LPS in a volume of 25 μl of sterile PBS.

pHrodo™-labeled *Pseudomonas aeruginosa* particle inoculation

Mice were anesthetized with isoflurane and intranasally infected with 4x10⁷ particles in a volume of 50 μl of sterile PBS and sacrificed 4h after.

***Pseudomonas aeruginosa* infection**

Pseudomonas aeruginosa was subcultured in tryptic soy broth for 3 hours at 37°C before injection, washed with sterile PBS, OD600 recorded and resuspended in PBS. Injected colony forming units (CFU) were retrospectively confirmed in counts of serial dilutions on blood agar plates. Mice were anesthetized with isoflurane and intranasally infected with stated concentration in a total volume of 50 μl (2x25μl).

Bronchoalveolar lavage (BAL)

Mice were anesthetized with isoflurane. The trachea was exposed and cannulated with 20G catheter. 1 ml of PBS (4°C) was gently infused followed by aspiration. This was repeated 5 times and total volume was recovered.

Bacterial load assay

CFU were determined by plating titrated amounts of lung homogenate or BAL on blood agar plates. Briefly, lung and BAL were harvested at indicated times post-infection. Tissue homogenates were generated by pushing the tissue through a 70 mm cell strainer using the plunger of a 5 ml syringe. Titrated 10-fold dilutions of tissue homogenate and BAL were serially diluted in PBS, plated on blood agar plates, and grown overnight at 37 °C.

In vitro pHrodo™ assay

100 μ l whole blood was incubated with 5 μ l of pHrodo™ Red E. coli BioParticles™ (Thermo Fisher Scientific, P35361) for 30 minutes at 37°C.

Cell isolation and flow cytometry

Blood was collected and lysed with RBC buffer (Biolegend) twice. After transcardiac perfusion with PBS (Thermo Fisher Scientific), solid organs were harvested, minced, and digested in a mixture of 450 U ml⁻¹ collagenase I, 125 U ml⁻¹ collagenase XI, 60 U ml⁻¹ DNase, and 60 U ml⁻¹ hyaluronidase (Sigma-Aldrich) in PBS on a shaker (800rpm) at 37°C for 20min (liver and pancreas), or 1 h (white/brown/mesenteric adipose tissue, skeletal muscle, heart and lung). Afterwards, the digested organ was flushed through a 40- μ m cell strainer. Spleens were pressed through a 40- μ m cell strainer and lysed with RBC. Peyer's patches and lymph nodes were pressed through a 40- μ m cell strainer. Bone marrow cells were flushed from the bone marrow cavities and brought into single-cell suspension by pipetting up and down, before lysis with RBC. Total viable cell numbers were counted using counting beads (Thermo Fisher Scientific). Small and large intestinal lamina propria was isolated as follows: after excision of the intestine, the Peyer's patches were removed under a microscope and the gut was cut open longitudinally to wash off the lumen contents in HBSS buffer. The gut was then cut into 1–2-cm pieces and subjected to 3 \times dissociation in EDTA-containing buffer (7.5 mM HEPES, 2% FCS, 2 mM EDTA, 10,000 U ml⁻¹ penicillin–streptomycin, 50 μ g ml⁻¹ gentamycin in HBSS; all Thermo Fisher Scientific) in a shaker at 37 °C for 15 min. After dissociation the epithelial layer was isolated (by filtering through a mesh) and discarded and the lamina propria digested in a mixture of 1M CaCl₂ (Sigma), 60 U/ml Dnase I, 5mg/ml Liberase TM (Roche), RPMI with L-Glutamin (Corning), 10% FCS, 5 mM Sodiumpyruvat (Corning cellgro), 5 mM HEPES (1M), 1% Pen/Strep. at 37°C for 40min. Single-cell suspensions were stained in FACS buffer (0.5% BSA and 2mM EDTA in PBS) containing fluorophore-coupled antibodies at a concentration of 1:700 at 4 °C for 20 min, unless otherwise indicated. To differentiate between live and dead cells, the cell suspensions were stained with Zombie Aqua (BioLegend) at a concentration of 1:1,000 in PBS at 4 °C for 15 min or by adding propidium iodide directly before flow cytometry analyses.

Cells were identified as

- (1) Ly-6C^{hi} monocytes (CD45+Lin1–CD11b+CD115+CX3CR1+F4/80–MHCII–Ly-6C^{hi}),
- (2) Ly-6C^{lo} monocytes (CD45+Lin1–CD11b+CD115+CX3CR1+F4/80–MHCII–Ly-6C^{lo}),
- (3) neutrophils (CD45+Lin1–CD11b+CX3CR1–Ly-6G+),
- (4) B cells(CD45+Lin1+CD11b–MHCII+),
- (5) T cells (CD45+Lin1+CD11b–MHCII–)
- (6) LSK cells (CD45+Lin2–Kit+Sca1+),
- (7) common myeloid progenitor (CD45+Lin2–Kit+Sca1–CD34+CD16/32^{mid}),
- (8) granulocyte–macrophage progenitor (CD45+Lin2–Kit+Sca1–CD34+CD16/32^{high}CD115–),
- (9) monocyte–dendritic cell progenitor (CD45+Lin2–Kit+Sca1–CD34+CD16/32^{high}CD115+); for neutrophil populations
- (10) Macrophages (CD45+CD11c–CD11b+Ly6G–MHCII+CD64+)
- (11) Lineages were defined as Lin1: CD3, CD90.2, CD19, NK1.1 and Lin2: B220, CD19, CD49b, Ter119, CD90.2, CD11b, CD11c, Ly-6G, IL-7R α . Data were acquired on a LSRII (BD Biosciences) and Cytex Aurora (Cytex). Data was analyzed with FlowJo (Tree Star)

RNA extraction and cDNA

PCR: Total RNA was isolated using the RNeasy Mini Kit (Qiagen, Venlo, Netherlands) according to the manufacturer's instructions. RNA quality and quantity were determined using NanoDrop (Thermo Fisher Scientific). cDNA was generated from a max. of 1 μ g of total RNA per sample using High Capacity cDNA Reverse Transcription Kit (Applied Biosystems). The High Capacity cDNA Reverse Transcription Kit (Applied Biosystems) was used to generate cDNA from up to 1 μ g of total RNA per sample.

Corticosterone ELISA

Plasma corticosterone concentrations were measured using a commercial corticosterone ELISA kit (Abcam, ab108821) following the manufacturer's instructions.

Chitinase 3-like 3 ELISA

Chi3l3 was measured in blood plasma and BAL supernatant using a self-coating ELISA kit (R&D Systems, DY2446).

Interleukin-6 ELISA

Mouse IL-6 Quantikine ELISA Kit (R&D Systems, M6000B) was used, following the manufacturer's instructions.

TNF-alpha ELISA

Mouse TNF-alpha Quantikine ELISA Kit (R&D Systems, MTA00B) was used, following the manufacturer's instructions.

Free Fatty Acid Quantitation Kit

Free fatty acids in plasma were measured, following the manufacturer's instructions (Sigma-Aldrich, MAK044).

Bulk RNA-seq

For bulk RNA sequencing, blood Ly-6C^{hi} monocytes (each sample pooled from n=5 mice) were FACS sorted (CD45⁺; Lin⁻; CD11b⁻; Ly-6G-CXCR1+Ly-6C⁺) into empty 1.5 mL tubes (4 mice pooled per sample, n=3 samples per group (fed vs. fasted+re-fed), total of n=24 mice). After centrifugation, the supernatant was removed and the cell pellet was lysed in RLT lysis buffer, from the RNeasy Micro Kit (Qiagen). The RNeasy Micro Kit (Qiagen) was subsequently used to extract the RNA following the manufacturer's instructions. RNA-seq libraries were constructed from total RNA using Clontech SMARTer v4 kit (Takara), followed by sequencing on an Illumina HiSeq 2500 instrument, resulting in 20-30 million 50 bp reads per sample. FASTQs files were processed by nf-core rnaseq pipeline with star_salmon configuration,⁴⁷ including multi QC,⁴⁸ alignment to the mm10 genome using STAR aligner⁴⁹ and counted using unstranded count function per gene_biotype feature by Salmon⁵⁰ using reference mouse gene models in standard GFF format. Downstream processing, including count normalization and differential gene expression analysis is conducted using the DESeq2⁵¹ applying a generalized linear model with the Wald statistical test under the assumption that underlying gene expression count data are distributed as a negative binomial distribution. Pathway enrichment analysis is done using clusterProlifer⁵² following the standard analytical procedures as described for fastGSEA algorithm⁵³. RNA sequencing data and unnormalized counts will be deposited for public access in the NCBI GEO database prior to publication of this manuscript.

Single-cell RNA-seq

For single-cell RNA sequencing, blood Ly-6Chi monocytes were FACS sorted (CD45⁺; Lin⁻; CD11b⁻; Ly-6G-CXCR1+Ly-6C⁺) into 1.5 mL tubes (5 mice pooled per sample, n=1 sample per group (fed vs. fasted+re-fed), total of n=10 mice). After cell counting and viability control, 6,601 (fed) and 7,560 (re-fed) cells were subjected to a single-cell RNA-seq. The library was constructed on the Chromium 10x instrument using Chromium single cell 3' reagent v3.0 kits, followed by sequencing on Illumina HiSeq 2500 instruments, which resulted in approximately 205-209 million reads per sample. FASTQs files were aligned to the mm10 genome provided from 10x (refdata-gex-mm10-2020-A. Alignment, filtering, barcode counting, UMI counting and identification of cells was performed with cellranger version 6.1.2. Count matrices were done aggregated using cellranger aggr with no normalization applied. Low quality cells identified by having less than 200 genes and dying cells with greater than 20% mitochondrial content were filtered out. Seurat was used for subsequent downstream analysis.⁵⁴ Each sample was independently normalized by dividing the gene count for each cell by the total counts of the cell, multiplied by a factor 10,000 and natural log transformed. Variable genes that were common across all samples was used as anchors for integration. Principal Component Analysis (PCA) was performed and the first 30 components were used for calculating the Uniform Manifold Approximation and Projection (UMAP) coordinates and k-nearest neighbors. The Louvain algorithm was used to construct the Shared nearest neighbor (SNN) graph with a resolution of 0.5. Marker genes were identified for each cluster Wilcoxon Rank Sum test. Trajectory and pseudotime inference were performed by Monocle3.⁵⁵ Clusters enriched in red blood cells as well as those enriched in mitochondrial and housekeeping genes were excluded first, before running clustering again using the leiden algorithm. The clustering algorithm from monocle3 also outputs 2 "partitions" of the data, and we keep the partition with the largest amount of cells to build one trajectory graph using reversed graph embedding. Cluster 7 from monocle's clustering was chosen as the root node to order the cells according to pseudotime.

QUANTIFICATION AND STATISTICAL ANALYSIS

Results are shown as mean \pm SEM. Statistical tests included unpaired, 2-tailed nonparametric Mann-Whitney tests (when Gaussian distribution was not assumed). For multiple comparisons, nonparametric multiple comparisons test comparing mean rank of each group (when Gaussian distribution was not assumed) or 1-way ANOVA followed by Tukey's test were performed. Survival was assessed by Log-rank (Mantel-Cox) test. P values of 0.05 or less were considered to denote statistical significance.